



Facial shape-from-shading: insights from directional statistics and neuroimaging

Edwin Hancock

Royal Society Wolfson Research Merit Award Holder

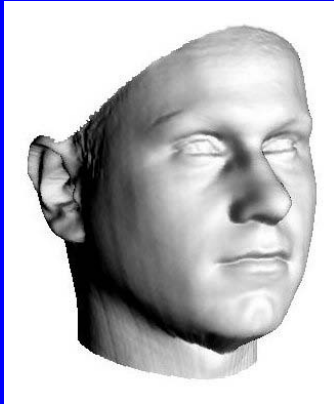
Department of Computer Science,
University of York, UK.

...joint work with Will Smith



The Image Formation Process

- Intrinsic features:



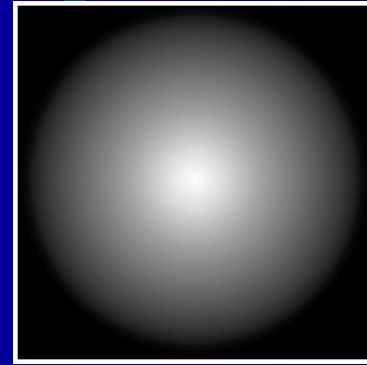
Shape

+



Texture/Albedo

+



BRDF

- Extrinsic parameters:

+

Lights (position, colour, direction)

Viewpoint and viewing direction

=



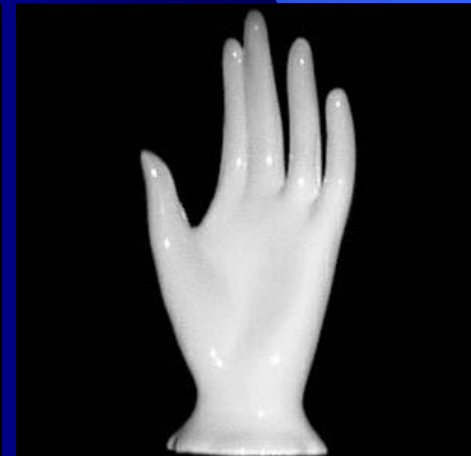
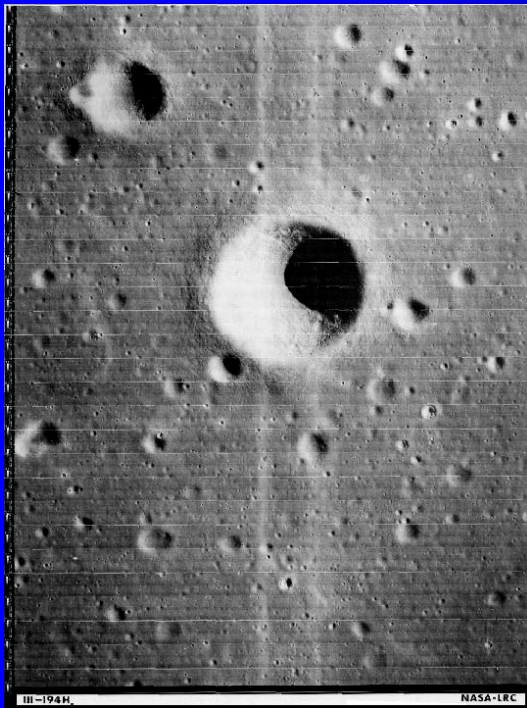
Image

Graphics and vision in inverse relationship

- Graphics: select albedo map and reflectance function to expedite realistic synthesis.
- Computer vision: analyse image contents to recover shape and texture (albedo) using assumed reflectance model.

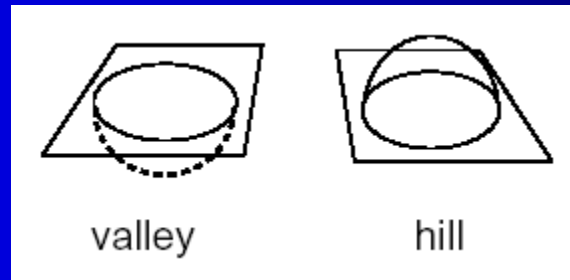
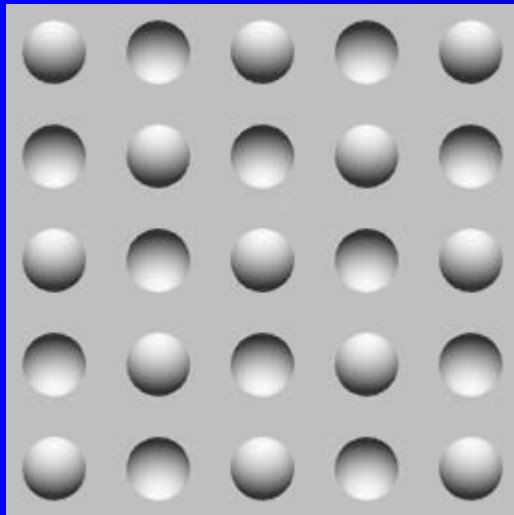
Shape-from-shading

- Photoclinometry, inverse-rendering
- 3D shape from a single image
- Shading conveys surface orientation and material properties



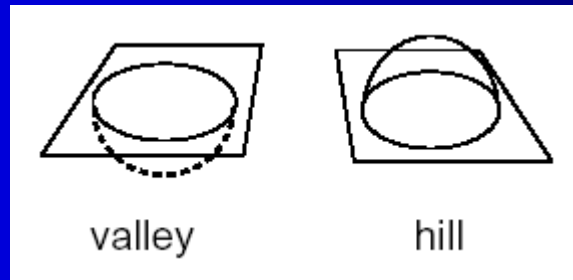
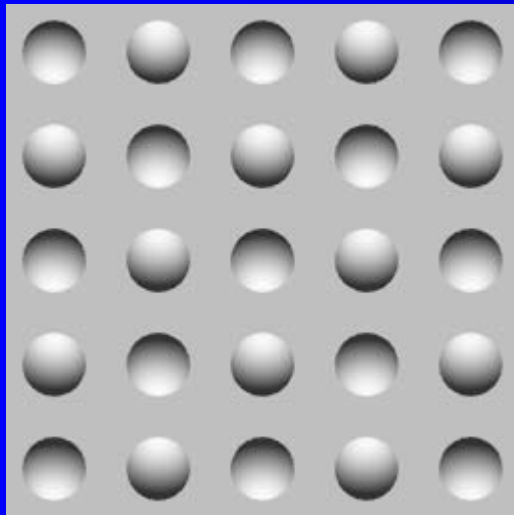
SFS in Humans

- Humans can perform shape-from-shading well
- Incorporate assumptions to help solve the problem



SFS in Humans

- Humans can perform shape-from-shading well
- Incorporate assumptions to help solve the problem



Facial SFS in Humans

- Assumptions can be overridden when interpretation would be inconsistent with prior knowledge



Facial SFS in Humans

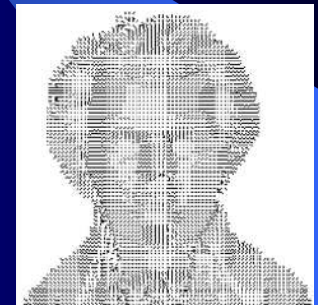
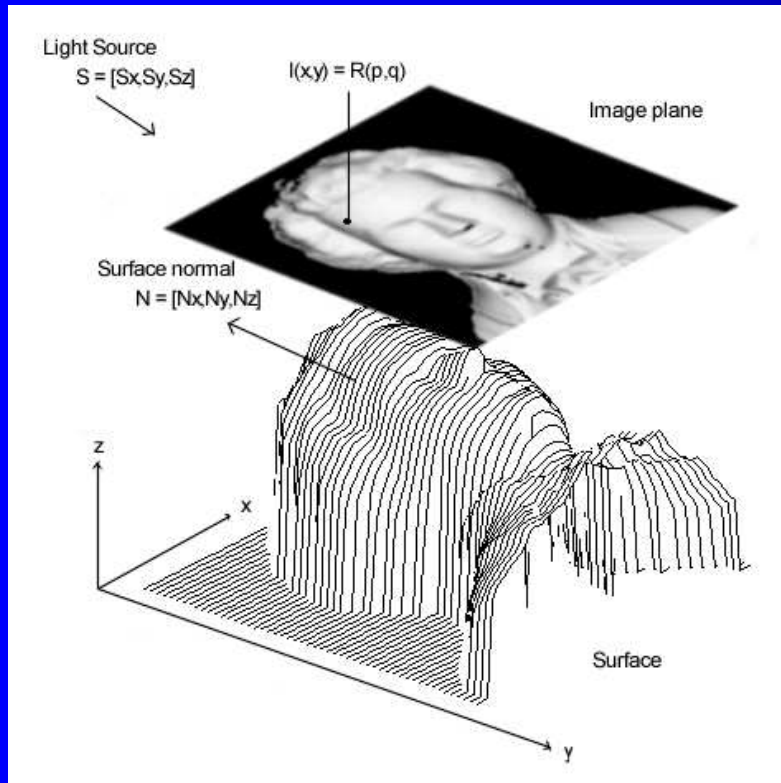
- Assumptions can be overridden when interpretation would be inconsistent with prior knowledge



- This motivates developing class-specific approaches

Shape from Shading

Overview



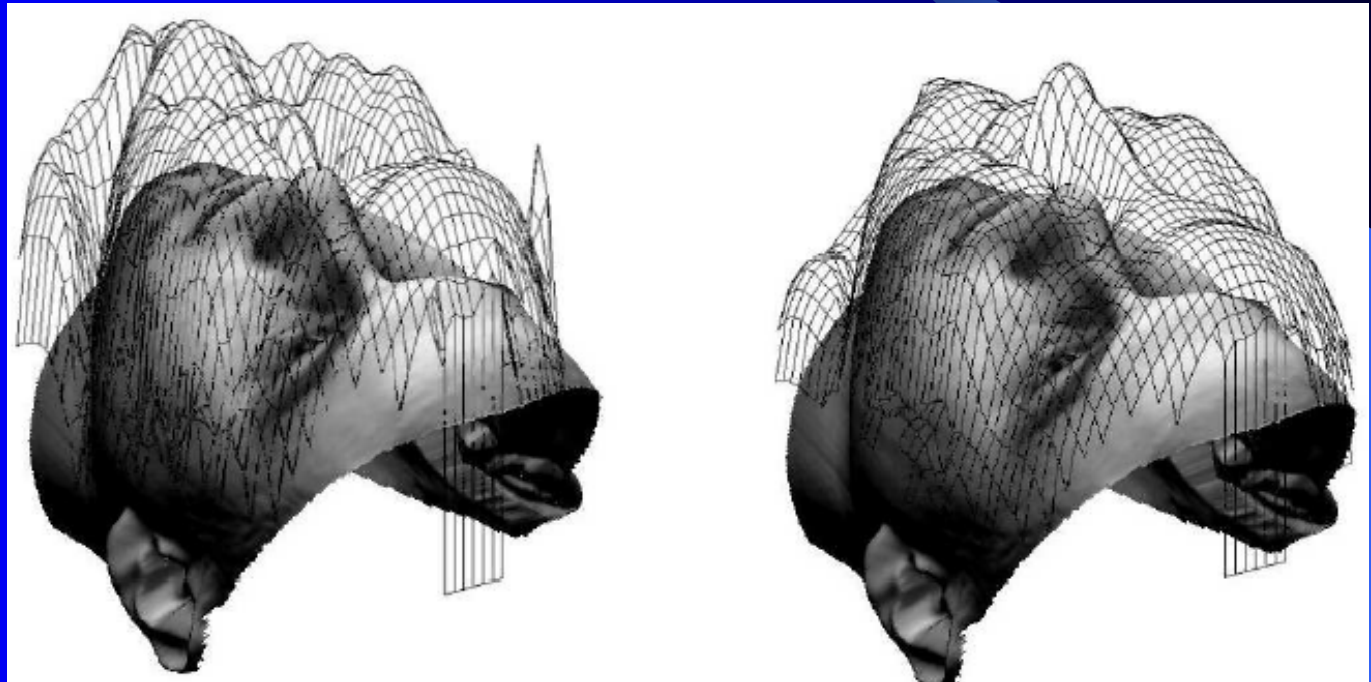
$$E(x, y) = R(p(x, y), q(x, y))$$

$$E(x, y) = \rho N \cdot S$$

$$N(x, y) = \frac{1}{\sqrt{1 + p(x, y)^2 + q(x, y)^2}} (p(x, y), q(x, y), 1)^T$$

Problem with SFS

Convex-concave ambiguities result in implosions of facial features



Aim in talk

- Use statistical model to recover facial shape without problems associated with concave-convex ambiguity.
- Estimate the intrinsic facial texture (albedo map) when shadowing present.
- Use reconstructions to test neural representation of faces via brain imaging experiments.

Papers

- Smith and Hancock, IEEE PAMI 2006.
- Ewbank, Smith, Hancock and Andrews, Cerebral Cortex, 2008.

Statistical Model for Facial Shape-from-shading

Model couched in surface
normal domain

A decorative graphic element consisting of a blue gradient shape that starts as a thin wedge and expands into a larger, curved area, resembling a stylized 'C' or a sector of a circle, positioned in the lower right portion of the slide.

Recovering facial shape from single images

- Many attempts to apply classical shape-from-shading methods to faces.
- Appealing since the surface height function can be recovered using a single image (under controlled lighting).
- However solution has been elusive since practical obstacles include concave/convex ambiguity, variable albedo and self-shadowing.

....also problems with albedo variations and shadows



.....devil resides in the detail

An abstract graphic design featuring a solid blue background. In the lower right quadrant, there is a large, light blue, curved shape that resembles a stylized 'C' or a partial circle. This shape is bordered by a darker blue area that tapers to a point on the left, creating a dynamic, angular composition.

Approach

- Extend point-distribution models to surface normals, and use them to represent variations in surface shape.
- Train model using data from a range sensor and fit it to brightness data using constraints provided by Lambert's law.
- Recovered 3D surface can be used for recognition (e.g. biometric analysis) or synthesis (generating avatars etc).

Methological contribution

Statistical modelling of surface orientation data is problematic since angle differences are not meaningful.

Use ideas from cartography to develop Cartesian representation of surface normal data.

Use representation to learn distribution of face shape and show how to fit model to image data using constraints provided by Lambert's law (model-based shape-from-shading). Solves problems with concave-convex inversion.

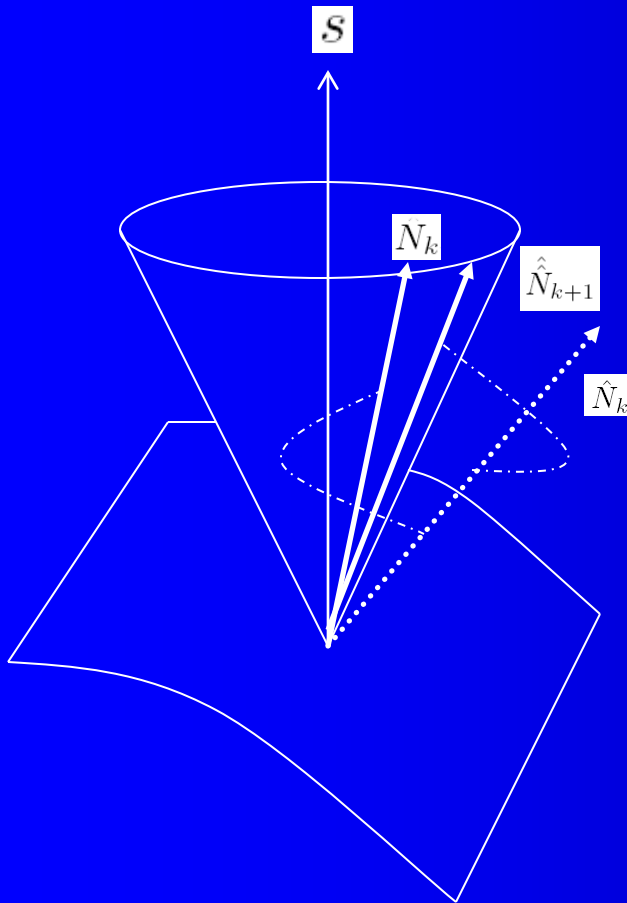
Geometric Shape-from-shading

Develop a geometric framework for shape-from-shading (Worthington and Hancock, PAMI 99 and PAMI 2001).

- Constrain surface normals to fall on cone with axis in the light source direction and apex angle $\arccos I$
- Use apparatus of robust statistics to develop a curvature sensitive method for surface normal smoothing.
- Initialise surface normals using the image gradient.
- Use resulting surface normal data to perform 3D object recognition from 2D images using surface curvature attributes. Also explore use of needle maps for view synthesis.

Geometric SFS

(Worthington and Hancock '99)



Surface normal must fall on a cone whose axis is light source direction and whose opening angle is determined by image brightness.

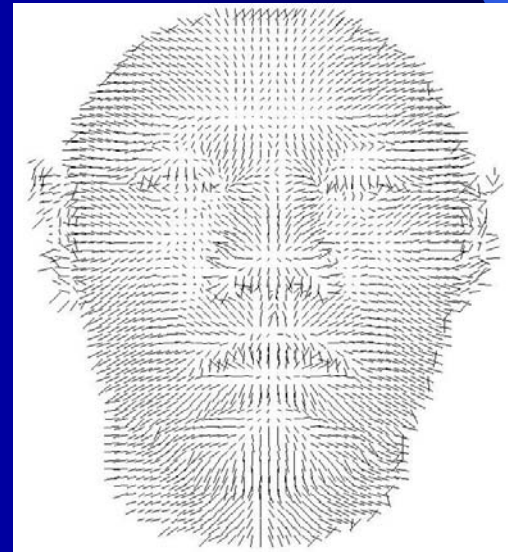
$$I = n \cdot s$$

Statistical model

A decorative graphic element in the bottom right corner of the slide. It consists of a light blue curved shape that tapers to a point, set against a darker blue background.

Statistical Surface Normal Model

- Our training data consists of an ensemble of K range scanned heads:
- We calculate a field of surface normals (a needle-map) from each sample:



Method

- Use range data to construct a statistical model for variations in surface orientation.
- Align range images and use gradient of range data to estimate surface normal directions
- Convert surface normal data into a convenient Cartesian form and apply PCA.
- Fit model to data so that it satisfies Lambert's law.
- Model imposes correct pattern of convexity/concavity on integrated field of surface normals.

Normals from range data

- Consider surface with height function

$$z = f(x, y)$$

- Consider a point on the surface where the unit surface normal is n .

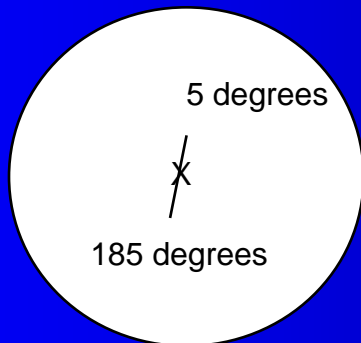
$$n = \frac{1}{\sqrt{1 + \left(\frac{\partial z}{\partial x}\right)^2 + \left(\frac{\partial z}{\partial y}\right)^2}} \begin{pmatrix} \frac{\partial z}{\partial x} \\ \frac{\partial z}{\partial y} \\ 1 \end{pmatrix}$$

Statistical model for surface normals

- Angular data is more difficult to model statistically than Cartesian data.
- Problem arises from angle wrap-around, and means that angular variance statistics are not meaningful.
- Some work (e.g. Heap and Hogg) has extended PDM's to polar co-ordinates.

....problem with angles

Cant compute meaningful statistics from angular data. The reason for this is that a small change in the direction of a vector can be recorded as large change in angle.

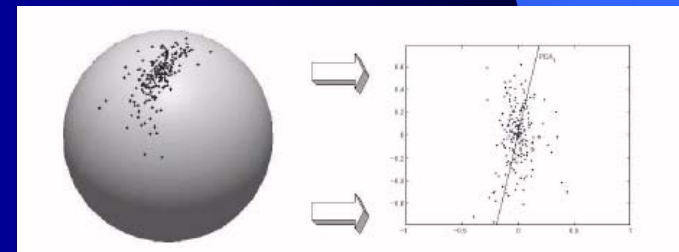
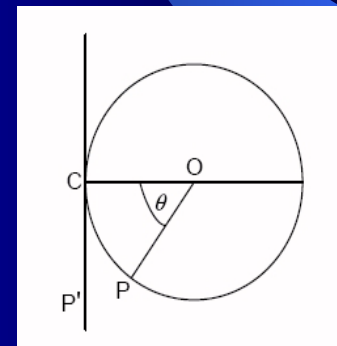


Example: Consider a short walk across the pole. The change in latitude is small, but small distances moved can give rise to very large changes in longitude,

Solution is to convert angular data to a sensible Cartesian form

Use ideas from cartography

- At each point on face represent distribution of surface normals from training data as points on a unit sphere. A surface normal is a point on the sphere.
- Use equidistant azimuthal projection to project points from sphere onto tangent plane to mean direction on sphere.
- Capture variations in face shape using point distribution on plane.



Equidistant azimuthal projection

At each image location the set of different surface normals in the training set is represented on a sphere of unit radius.

Co-latitude is zenith angle and longitude is azimuth angle of surface normal

Construct a tangent plane to the sphere at the point local mean surface normal direction.

Project points from sphere (surface normals) onto the tangent plane using the equidistant azimuthal projection.

Projection preserves the distance to the mean normal on the sphere.

Surface normals become points on the tangent plane.

Point-distribution model describes statistical properties of projected surface normals.

Equidistant azimuthal projection

At each image location the set of different surface normals in the training set is represented on a sphere of unit radius.

Co-latitude is zenith angle and longitude is azimuth angle of surface normal

Construct a tangent plane to the sphere at the point local mean surface normal direction.

Project points from sphere (surface normals) onto the tangent plane using the equidistant azimuthal projection.

Projection preserves the distance to the mean normal on the sphere.

Surface normals become points on the tangent plane.

Point-distribution model describes statistical properties of projected surface normals.

Equidistant azimuthal projection

At each image location the set of different surface normals in the training set is represented on a sphere of unit radius.

Co-latitude is zenith angle and longitude is azimuth angle of surface normal

Construct a tangent plane to the sphere at the point local mean surface normal direction.

Project points from sphere (surface normals) onto the tangent plane using the equidistant azimuthal projection.

Projection preserves the distance to the mean normal on the sphere.

Surface normals become points on the tangent plane.

Point-distribution model describes statistical properties of projected surface normals.

Equidistant azimuthal projection

At each image location the set of different surface normals in the training set is represented on a sphere of unit radius.

Co-latitude is zenith angle and longitude is azimuth angle of surface normal

Construct a tangent plane to the sphere at the point local mean surface normal direction.

Project points from sphere (surface normals) onto the tangent plane using the equidistant azimuthal projection.

Projection preserves the distance to the mean normal on the sphere.

Surface normals become points on the tangent plane.

Point-distribution model describes statistical properties of projected surface normals.

Equidistant azimuthal projection

At each image location the set of different surface normals in the training set is represented on a sphere of unit radius.

Co-latitude is zenith angle and longitude is azimuth angle of surface normal

Construct a tangent plane to the sphere at the point local mean surface normal direction.

Project points from sphere (surface normals) onto the tangent plane using the equidistant azimuthal projection.

Projection preserves the distance to the mean normal on the sphere

Surface normals become points on the tangent plane.

Point-distribution model describes statistical properties of projected surface normals.

Equidistant azimuthal projection

At each image location the set of different surface normals in the training set is represented on a sphere of unit radius.

Co-latitude is zenith angle and longitude is azimuth angle of surface normal

Construct a tangent plane to the sphere at the point local mean surface normal direction.

Project points from sphere (surface normals) onto the tangent plane using the equidistant azimuthal projection.

Projection preserves the distance to the mean normal on the sphere.

Surface normals become points on the tangent plane.

Point-distribution model describes statistical properties of projected surface normals.

Equidistant azimuthal projection

At each image location the set of different surface normals in the training set is represented on a sphere of unit radius.

Co-latitude is zenith angle and longitude is azimuth angle of surface normal

Construct a tangent plane to the sphere at the point local mean surface normal direction.

Project points from sphere (surface normals) onto the tangent plane using the equidistant azimuthal projection.

Projection preserves the distance to the mean normal on the sphere.

Surface normals become points on the tangent plane.

Point-distribution model describes statistical properties of projected surface normals.

From normals to angles

Mean surface normal at pixel (i,j)

$$\hat{n}(i, j) = \frac{\bar{n}(i, j)}{\|\bar{n}(i, j)\|}$$

$$\bar{n}(i, j) = \frac{1}{\#T} \sum_{k \in T} n_k(i, j)$$

Zenith and azimuth angles of surface normal

$$\theta(i, j) = \frac{\pi}{2} \arcsin n^z(i, j)$$

$$\phi(i, j) = \arctan \frac{n^y(i, j)}{n^x(i, j)}$$

The projection

$$x_k(i, j) = k' \cos \theta_k(i, j) \sin[\phi_k(i, j) - \hat{\phi}(i, j)] \quad (3)$$

$$y_k(i, j) = k' \left\{ \cos \hat{\theta}(i, j) \sin \phi_k(i, j) - \sin \hat{\theta}(i, j) \cos \theta_k(i, j) \cos[\phi_k(i, j) - \hat{\phi}(i, j)] \right\} \quad (4)$$

where $k' = \frac{c}{\sin c}$ and $\cos c = \sin \hat{\theta}(i, j) \sin \theta_k(i, j) + \cos \hat{\theta}(i, j) \cos \theta_k(i, j) \cos[\phi_k(i, j) - \hat{\phi}(i, j)]$.

Encoding the projection

Encode the transformed co-ordinates as a long-vector for each training pattern

$$U^k = \begin{pmatrix} x_k(1,1) \\ y_k(1,1) \\ .. \\ x_k(M,N) \\ y_k(M,N) \end{pmatrix}$$

Training data must be very carefully aligned.

Stack long-vectors to form data matrix

$$D = (U^1 \mid U^2 \mid \mid U^k \mid \mid U^K)$$

Covariance matrix eigenvectors

Construct covariance matrix (long vectors have zero mean)

$$L = \frac{1}{K} DD^T$$

Locate eigenvectors of L by applying Sirovich snapshot method to

$$\hat{L} = \frac{1}{K} D^T D = \hat{\Phi} \Lambda \hat{\Phi}^T$$

Eigenvectors of L

$$\Phi = D \hat{\Phi}$$

Model parameters

The mean long-vector is the null-vector. Hence deformed field of EAP normals is deformed according to

$$\tilde{U} = \Phi b$$

Best fit parameter vector

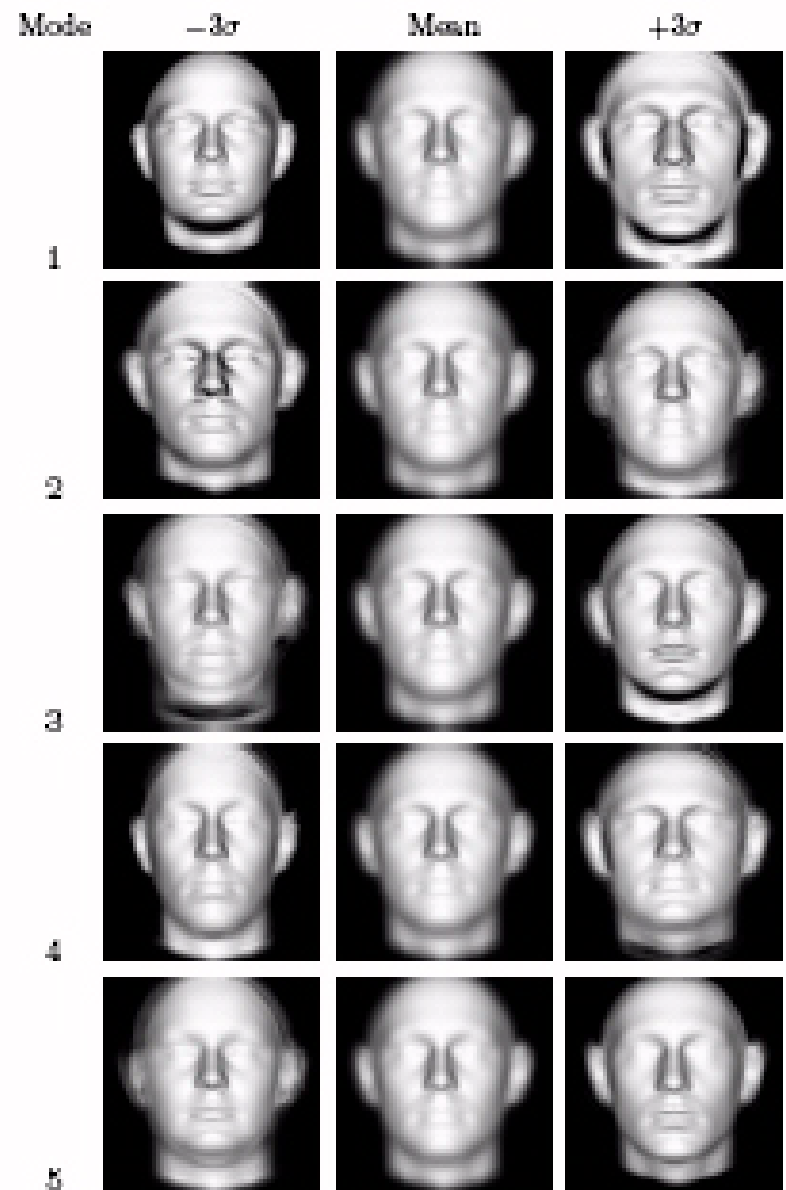
$$b = \Phi^T U$$

Data used for training

Max Plank Institute: collected with Cyberware 3030PS scanner; 100 males and 100 females. Data aligned using manual landmarks.

Learn model from laser range finder images

- Captures variations in face shape
- Displacements from average face.



Fitting the model to image brightness data and surface height recovery

Estimating shape-parameters
from brightness images

A decorative graphic element consisting of a blue gradient shape that starts as a thin wedge and expands into a larger, curved area, resembling a stylized arrow or a corner of a page.

Fitting algorithm

- Make an initial estimate of field of surface normals using SFS. Convert them to points using EAP.
- Find best fit model parameters. Recover best fit set of EAP co-ordinates. Transform best-fit co-ordinates back into polar representation (onto sphere) using inverse EAP. Gives field of surface normals.
- Rotate best-fit normals onto nearest location on irradiance cone. Resulting normals satisfy Lambert's law.
- Iterate model-fitting and cone-constraints until convergence is reached.

Fitting algorithm

- Make an initial estimate of field of surface normals using SFS. Convert them to points using EAP.
- Find best fit model parameters. Recover best fit set of EAP co-ordinates. Transform best-fit co-ordinates back into polar representation (onto sphere) using inverse EAP. Gives field of surface normals.
- Rotate best-fit normals onto nearest location on irradiance cone. Resulting normals satisfy Lambert's law.
- Iterate model-fitting and cone-constraints until convergence is reached.

Fitting algorithm

- Make an initial estimate of field of surface normals using SFS. Convert them to points using EAP.
- Find best fit model parameters. Recover best fit set of EAP co-ordinates. Transform best-fit co-ordinates back into polar representation (onto sphere) using inverse EAP. Gives field of surface normals.
- Rotate best-fit normals onto nearest location on irradiance cone. Resulting normals satisfy Lambert's law.
- Iterate model-fitting and cone-constraints until convergence is reached.

Fitting algorithm

- Make an initial estimate of field of surface normals using SFS. Convert them to points using EAP.
- Find best **fit model parameters**. Recover best fit set of EAP co-ordinates. Transform best-fit co-ordinates back into polar representation (onto sphere) using inverse EAP. Gives field of surface normals.
- Rotate best-fit normals onto nearest location on **irradiance cone**. Resulting normals satisfy Lambert's law.
- Iterate model-fitting and cone-constraints until convergence is reached.

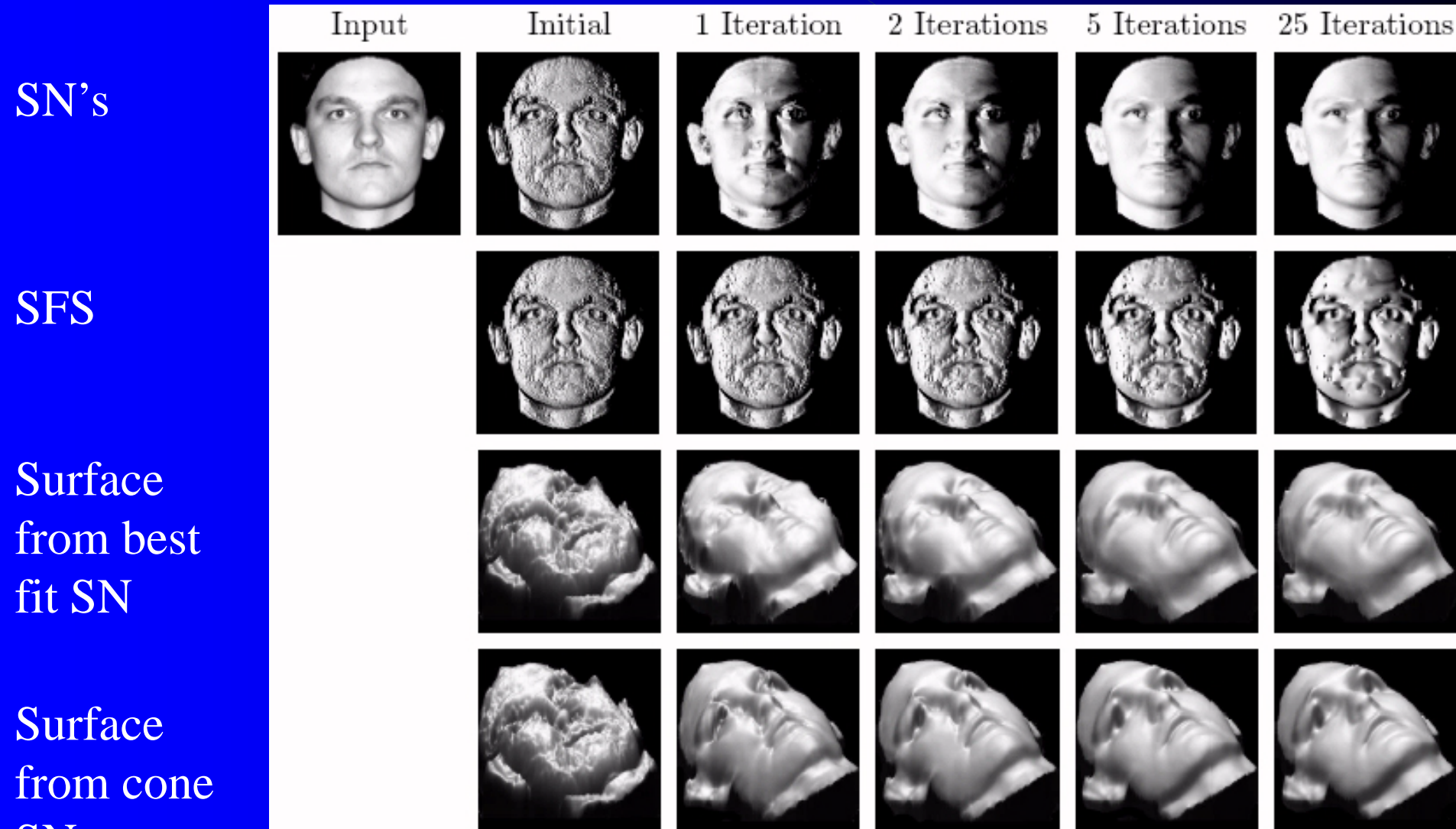
Surface recovery

.....use Frankot and Chellappa Fourier domain integration method.

However, surface heights can be modelled statistically using a coupled model (...later).

Iterative model fitting

- Overcomes problems of false concavities



Estimating albedo

A decorative graphic element consisting of a blue gradient shape that starts as a thin wedge and expands into a larger, curved area, resembling a stylized comet tail or a modern architectural element. It is positioned in the lower right quadrant of the slide.

Albedo estimation

Idea: At convergence differences between on-cone normals and best-fit normals measure departures from Lambert's law. Provided that there are no specularities present, these differences can be ascribed to variations in facial albedo.

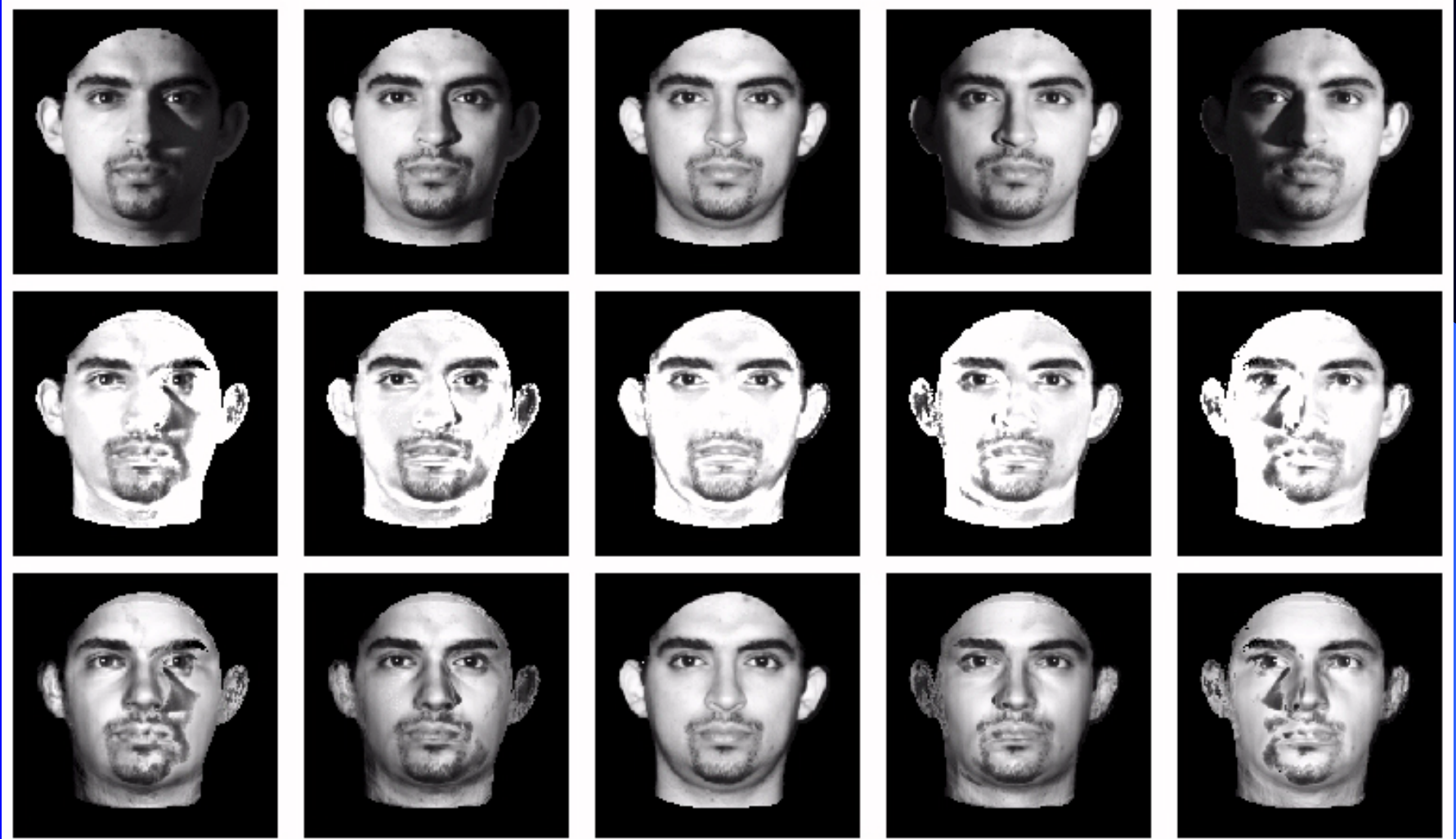
Albedo estimate

$$\rho = \frac{I}{n_{fit} \cdot S}$$

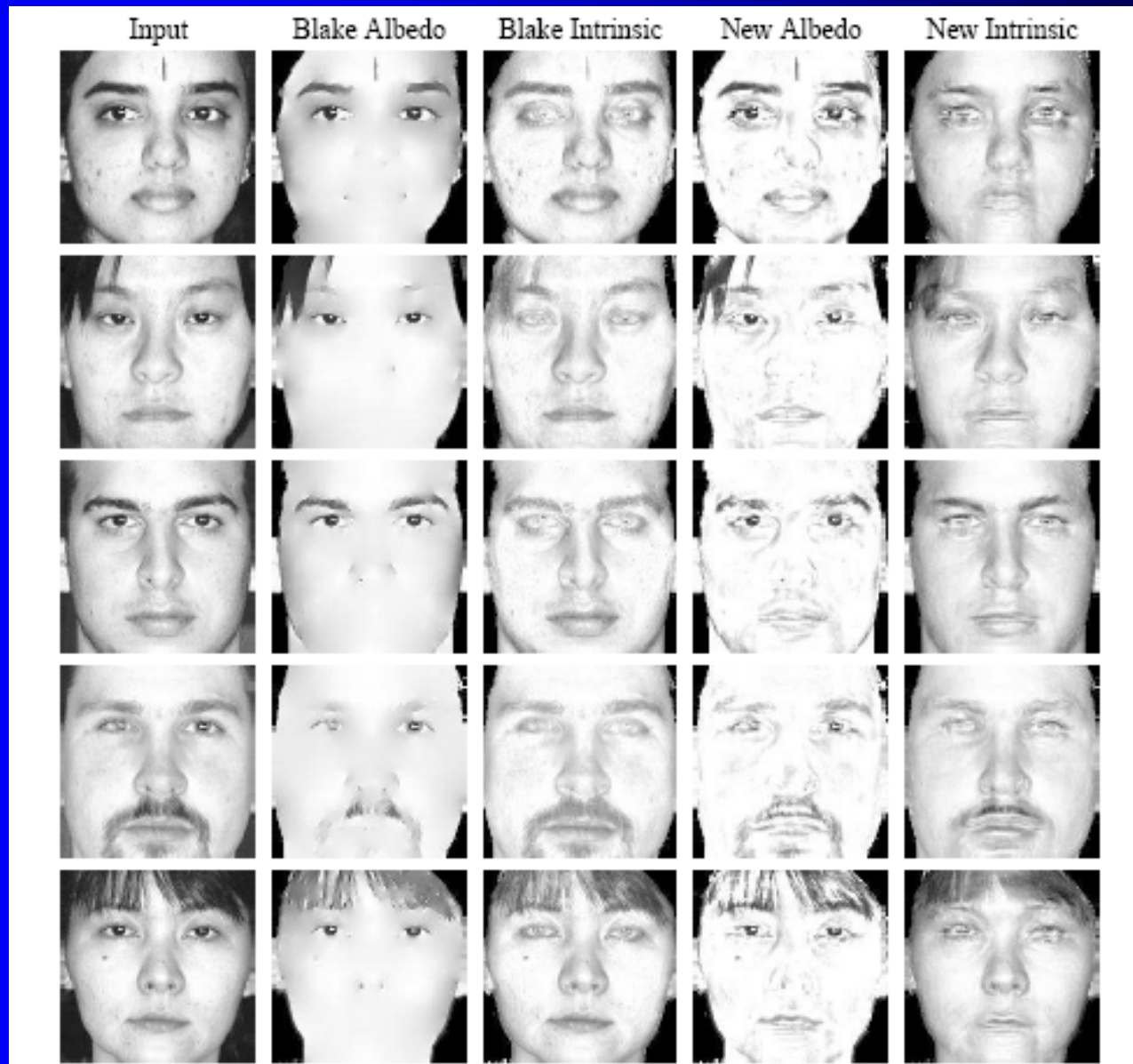
Difference between cone and fit normals



Albedo with varying illumination direction



Comparison with Blake's method



View synthesis

- Re-illuminate with Lambertian reflectance using estimated albedo map and variable light source:

$$I_{synth} = \rho_{est} n_{fit} \cdot s_{new}$$

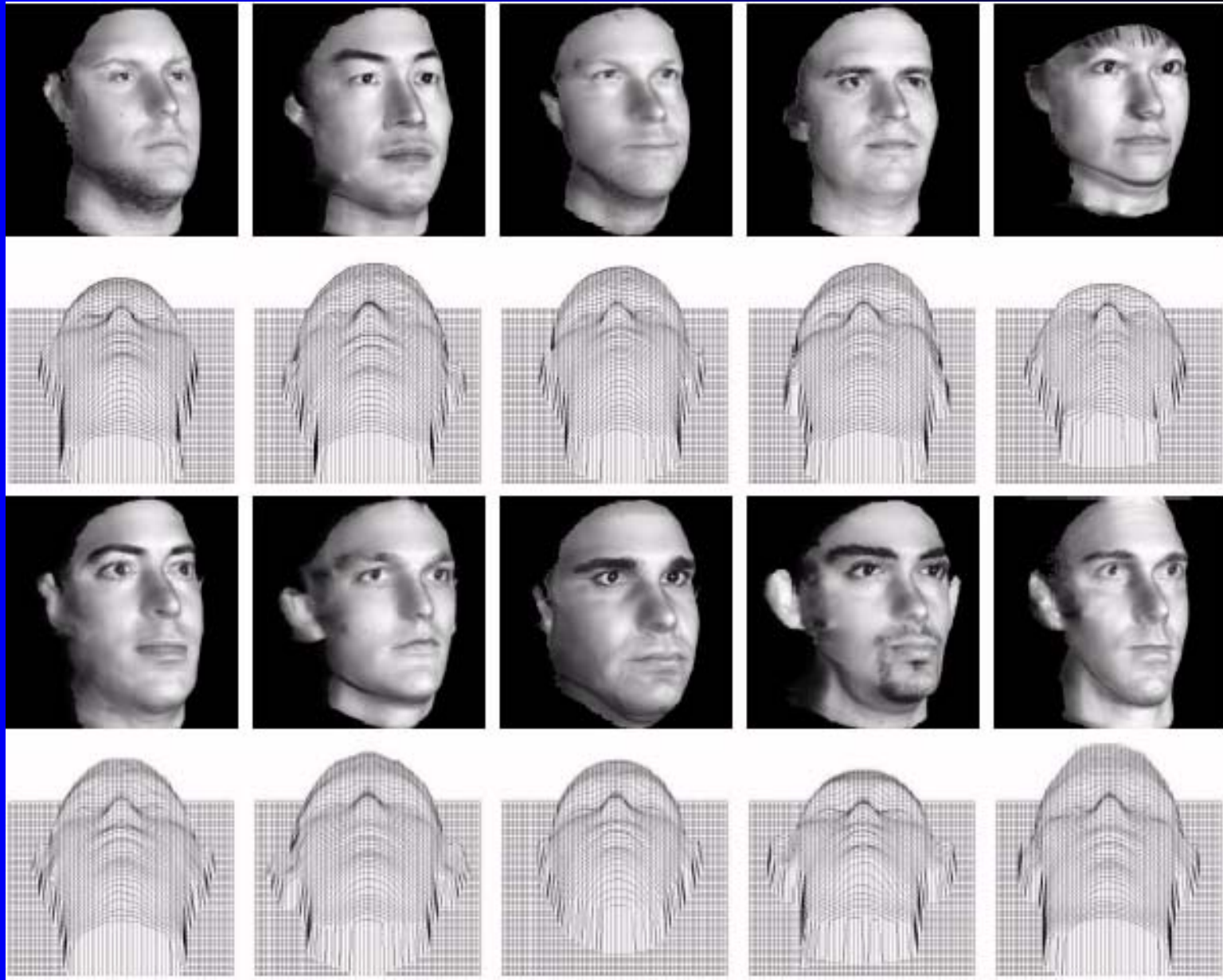
- Texture map onto surface reconstructed from surface normals using F+C integration method.
- Rotate rendered surface to obtain new poses.

View synthesis with variable illumination

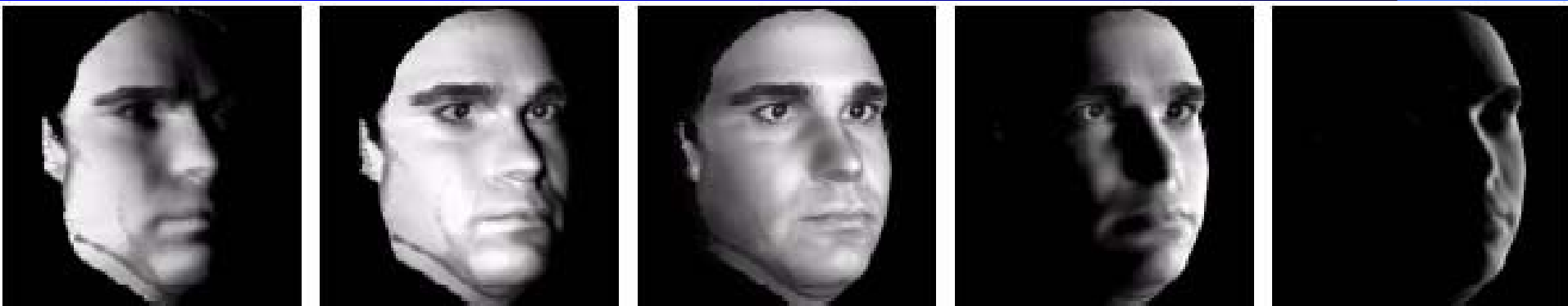


Orig. Alb.

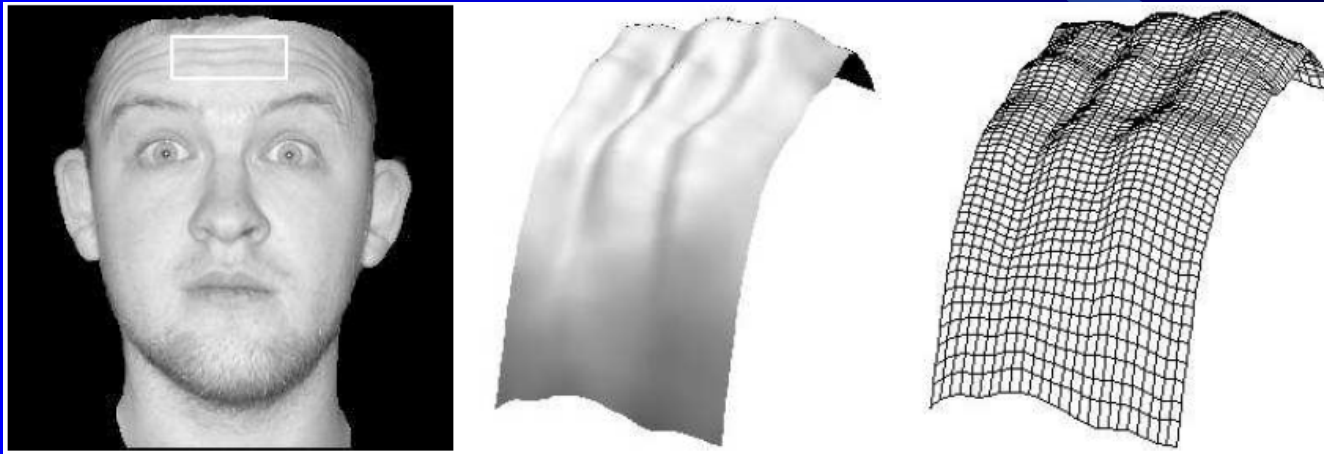
Rotated pose



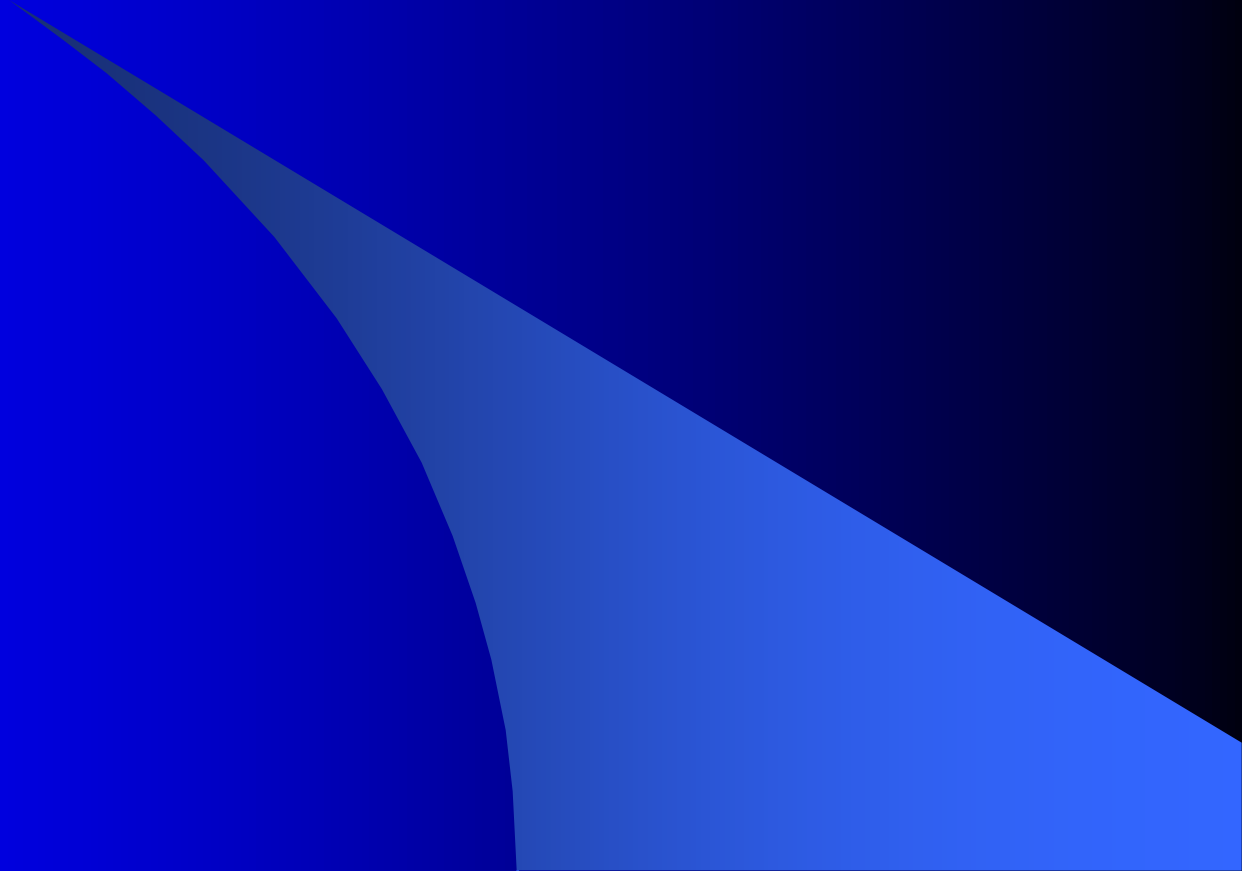
Pose and illumination varied



Recovery of Local Shape Features



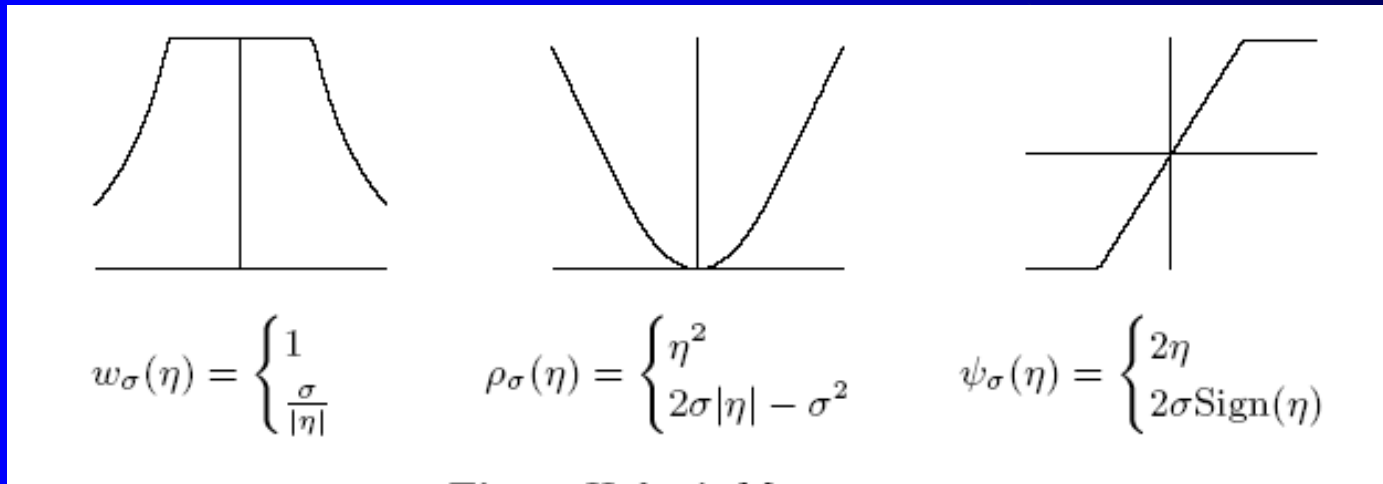
Dealing with self shadowing



Robust fitting and shadow maps

- Weight against pixels with poor brightness error.
- These are locations of shadows or severe image noise.
- Allows recovery of a shadow map.

Iterative robust estimation



Weighted estimate of
parameter vector

$$b^{(t)} = \Phi^T W^{(t)} U^{(t)}$$

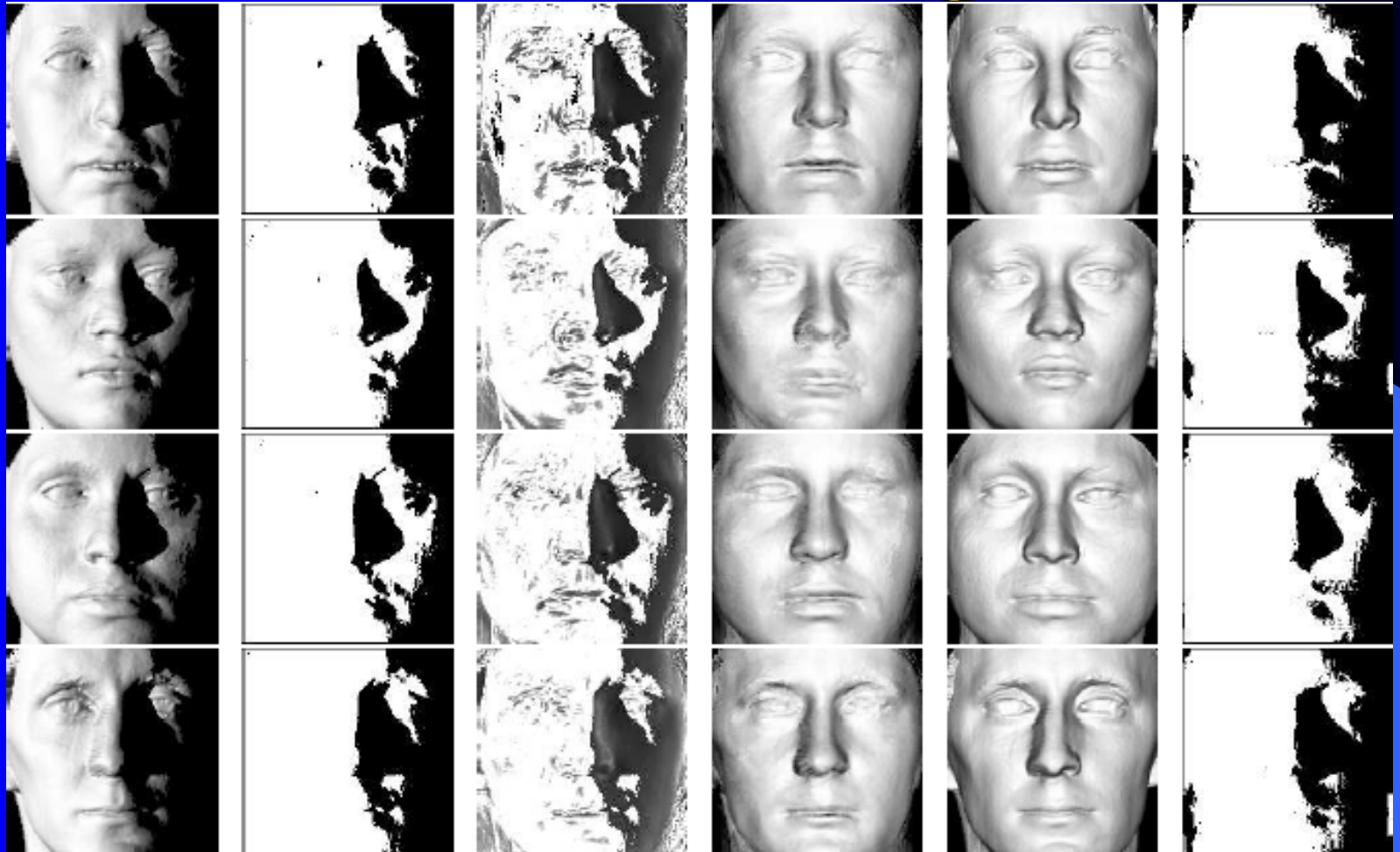
Weight matrix given by
error residuals

$$W^{(t+1)} = w_\sigma(\|U^{(t)} - \Phi^T b^{(t)}\|)$$

Shadow detection

- Perform surface integration to recover height function.
- For pixels with low weight, ray-trace from light source.
- If ray intersects surface, then pixel is in shadow.

Results of robust fitting



original

shadow

weights

Orig.

Robust

Est. shad.

Real world examples



Real world data: effect of light source direction

Input



Estimated
shadow map



Frontal
illumination



Varying light source direction

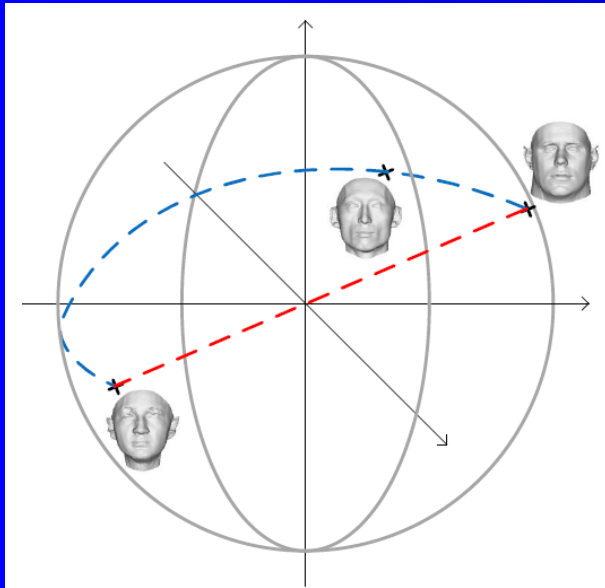
Recognition

- Use parameter vector b for recognition, augmented with facial albedo map.
- Competes with number of well known methods (harmonic bases, 9 points of light, etc).
- Can be used to perform gender classification and construct facial shape-spaces.

Shape spaces

- In parameter space, **direction** corresponds to **identity** and **length** corresponds to **distinctiveness**
- Identity or “space of plausible faces” forms a manifold – hyperellipse (or hypersphere if normalise dimensions by eigenvalues)

Geodesic or Euclidean steps?



Source:



Target:



Antiface:



Linear warp



Plausibility-preserving warp



Non-Euclidean data

- Arises when data is sampled from a manifold, rather than a Euclidean space.
- Examples include directional data (hyperspherical) and tensor-MRI (half-cone).
- Analysis tools limited (how to define mean and covariance or analyse modes of variance)

Non-metricity

- When characterised in terms of dissimilarities, data can display non-metric artefacts.
- Characterised by negative eigenvalues of the dissimilarity matrix.

Prior Work

- Pennec – developed framework for analysing statistics of data residing on a manifold.
- Ayache – uses methods to develop algorithms for analysis of tensor-MRI data.
- Joshi+Fletcher – develop manifold analogue of PCA – principal geodesic analysis.

Aims in this talk

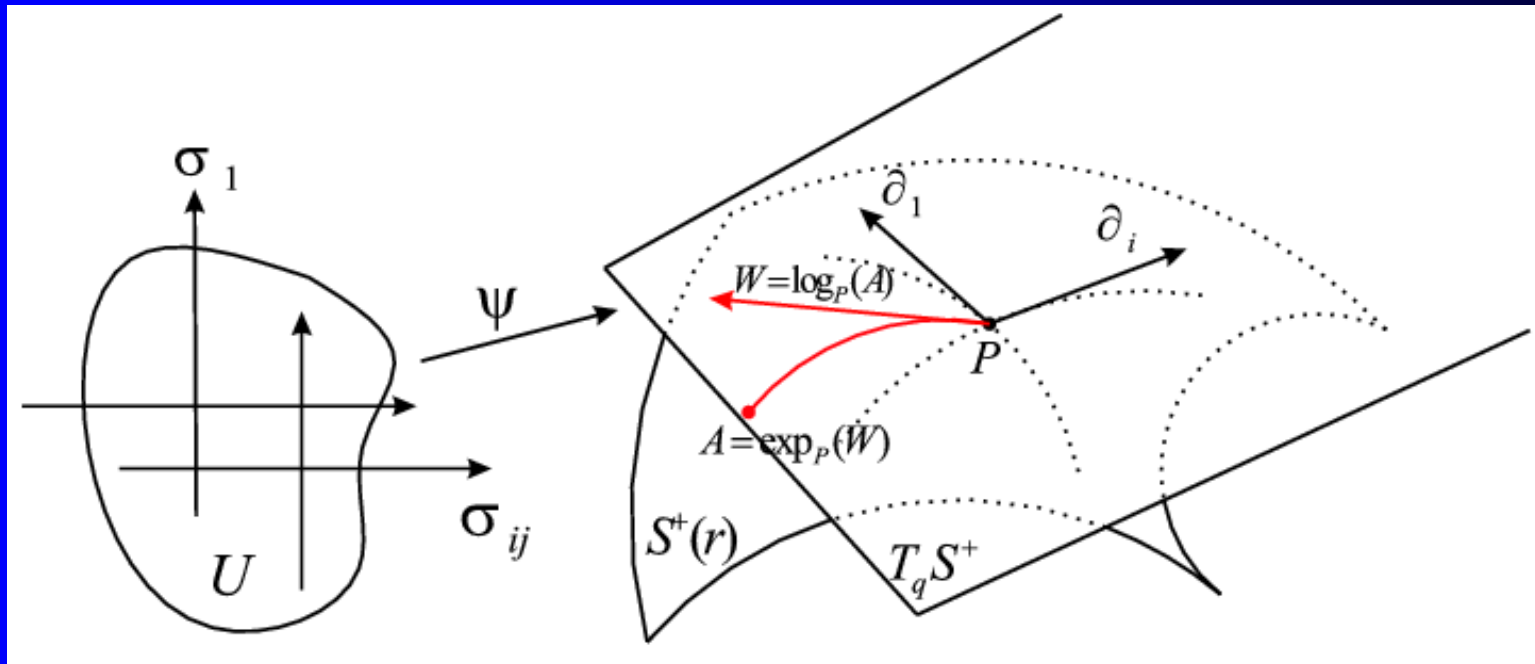
- Show how framework can be used to develop algorithms for analysis of directional data.
- Filtering and diffusion smoothing algorithms.
- Learning statistical shape-models.
- Classification and clustering.

Data on a manifold

Lie group representation

A decorative graphic element in the bottom right corner of the slide. It consists of a large, curved shape that transitions from a medium blue color on the left to a lighter blue color on the right, creating a gradient effect. The shape is abstract and modern, resembling a stylized 'C' or a portion of a circle.

Illustration of the geometry of the tensor space



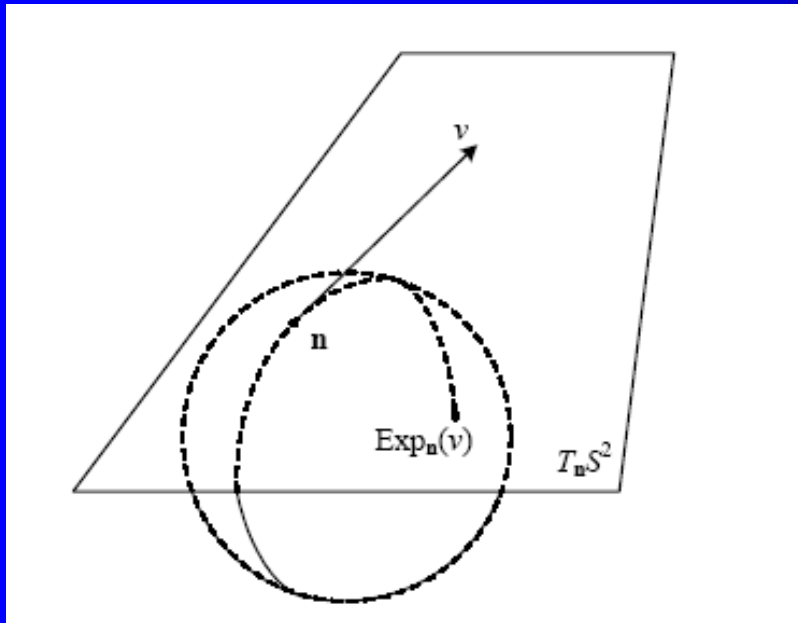
Local coordinate system, tangent space, exponential map and Logarithmic map at q of manifold M .

- **Exponential map:** takes points from manifold onto tangent plane so as to preserve geodesic distance. Euclidean distance on tangent-plane equals geodesic distance on manifold.
- **Logarithmic map** is inverse of exponential map. Puts points back on manifold, so that geodesic distance is equal to Euclidean distance on tangent plane.

Statistics on Riemannian Manifolds

Gives more elegant update algorithm (IJCV 2009).

Exponential map of surface normal distribution



Use **principal geodesic analysis** (Fletcher, Pizer) to develop compact needle map update equation:

.....strongly liked to recent work on statistics on Riemannian manifolds by Pennec and by Faugeras.

Spherical median

- Intrinsic mean

$$\mu = \arg \min_n \sum_i d(n, n_i)$$

- Recursive estimation

$$\mu^{(t+1)} = \text{Exp}_{\mu^{(t)}} \left(\frac{1}{K} \sum_{i=1}^K \text{Log}_{\mu^{(t)}}(n_i) \right)$$

Principal geodesic directions

- Leading geodesic:

$$v_1 = \arg \max_{\|v\|=1} \sum_i [v \operatorname{Log}_\mu(n_i)]^2$$

- Remainder found recursively

$$v_k = \arg \max_{\|v\|=1} \sum_i \sum_{j=1}^{k-1} \left(v_j \operatorname{Log}_\mu(n_i) \right)^2 + \left(v \operatorname{Log}_\mu(n_i) \right)^2$$

Model parameters using PGA

- Normals

$$n_p = \text{Exp}_{\mu_p}(\Phi b)_p$$

- Best fit parameter vector

$$b^* = \arg \min_b \| I - s.\text{Exp}_{\mu}(\Phi b) \|^2$$

- In terms of covariance matrix

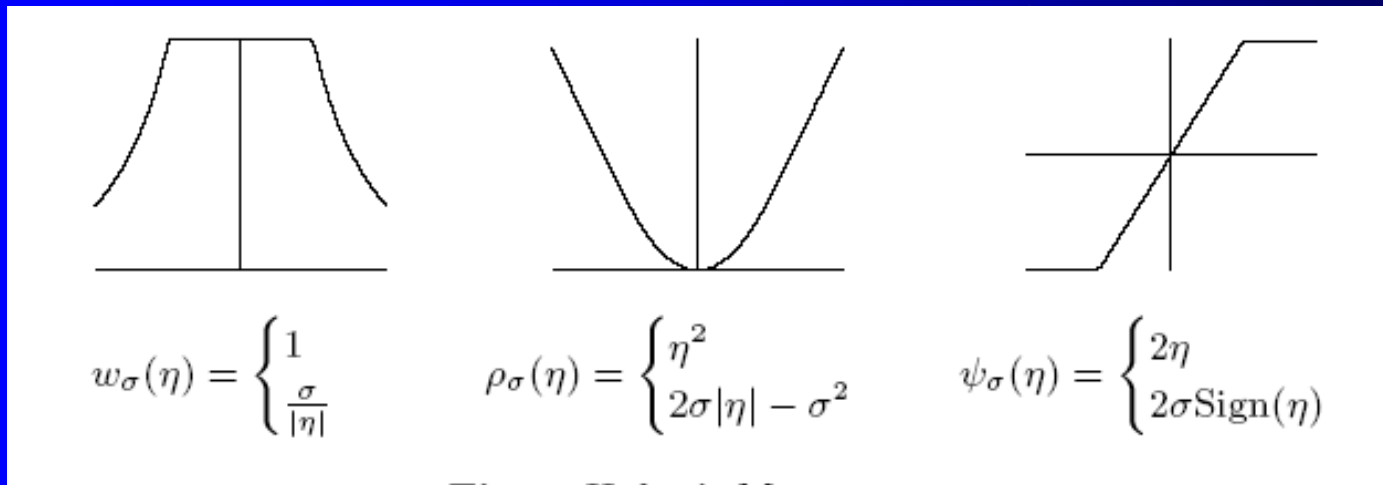
$$b = \Phi^T \text{Log}_{\mu}(N^{(t)})$$

Surface normal update

- Rotations onto irradiance cone become simple in terms of operations on exponential and logarithmic maps

$$n_p^{(t+1)} = \text{Exp}_s \left(\arccos I \frac{\text{Log}_s \left(\text{Exp}_\mu (\Phi b^{(t)})_p \right)}{\| \text{Log}_s \left(\text{Exp}_\mu (\Phi b^{(t)})_p \right) \|} \right)$$

Iterative robust estimation



Weighted estimate of
parameter vector

$$b^{(t+1)} = CP^T W^{(t)} \text{Log}_\mu(U^{(t)})$$

Weight matrix given by
error residuals

$$\eta_P^{(t)} = \| \text{Log}_{\mu_P}(n_p^{(t)}) = (Pb^{(t)})_p \|$$

Non-Lambertian reflectance

Allow for diffuse and specular reflection (IJCV 2010).

A decorative graphic element consisting of a blue gradient shape that starts as a thin wedge on the left and expands into a larger, curved triangular shape towards the bottom right corner of the slide.

Non-Lambertian SFS

- Faces do not strictly obey Lamberts law,
- Torrance and Sparrow reflectance model [Torrance&Sparrow 1967]

$$g_{T\&S}(N, L, V, \{\rho_d, \rho_s, \nu, L\}) \\ = L\rho_d N \cdot S + L\rho_s \exp(-\nu^2 \arccos(N \cdot \frac{L+V}{\|L+V\|})^2) / (N \cdot V)$$

- Brightness error

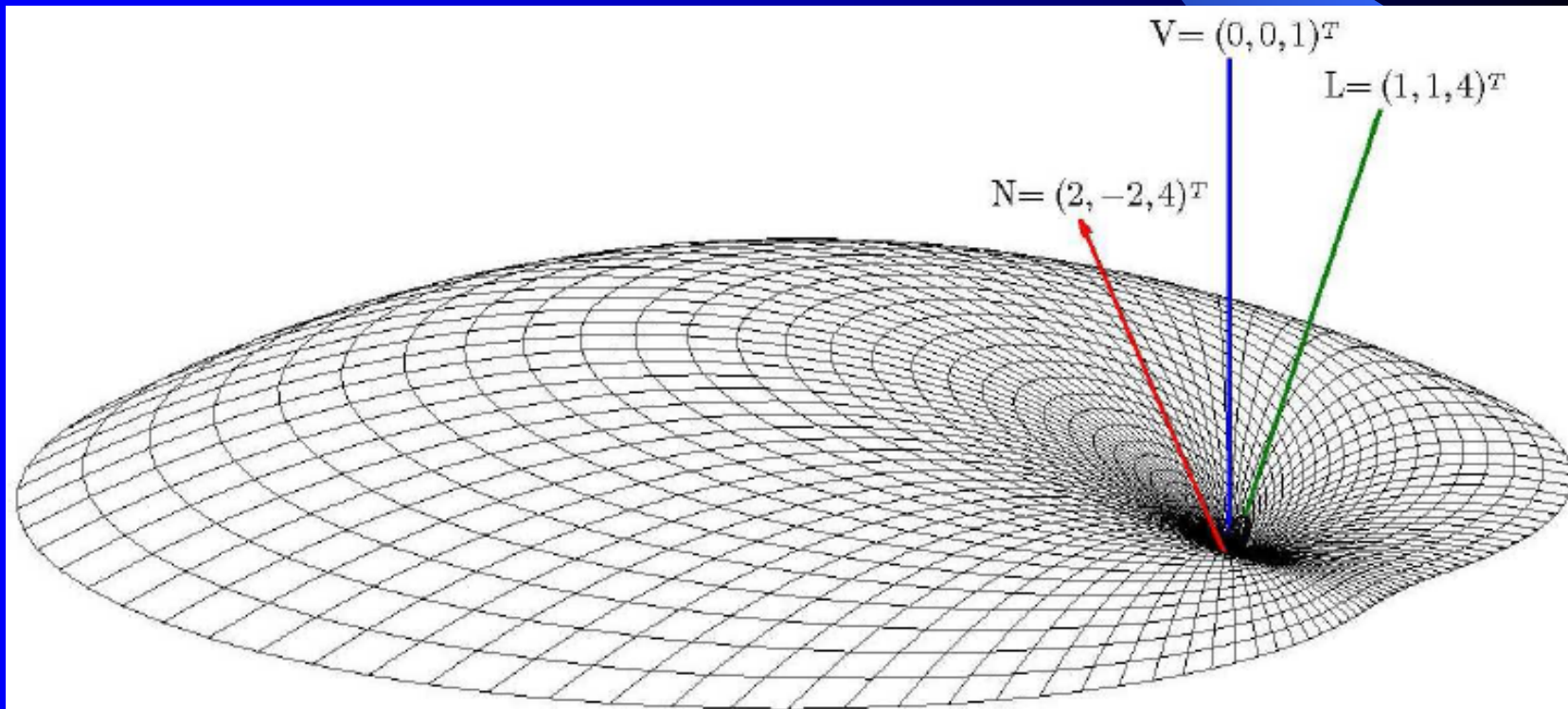
$$f(n) = (g(\Phi(n), L, V, \{\rho_d, \rho_s, \nu, L\}) - I)^2$$

- Gradient descent is used to locate the surface normal minimizing the brightness error:

$$n_{t+1} = \text{Exp}_{n_t}(-\gamma \nabla f(n_t))$$

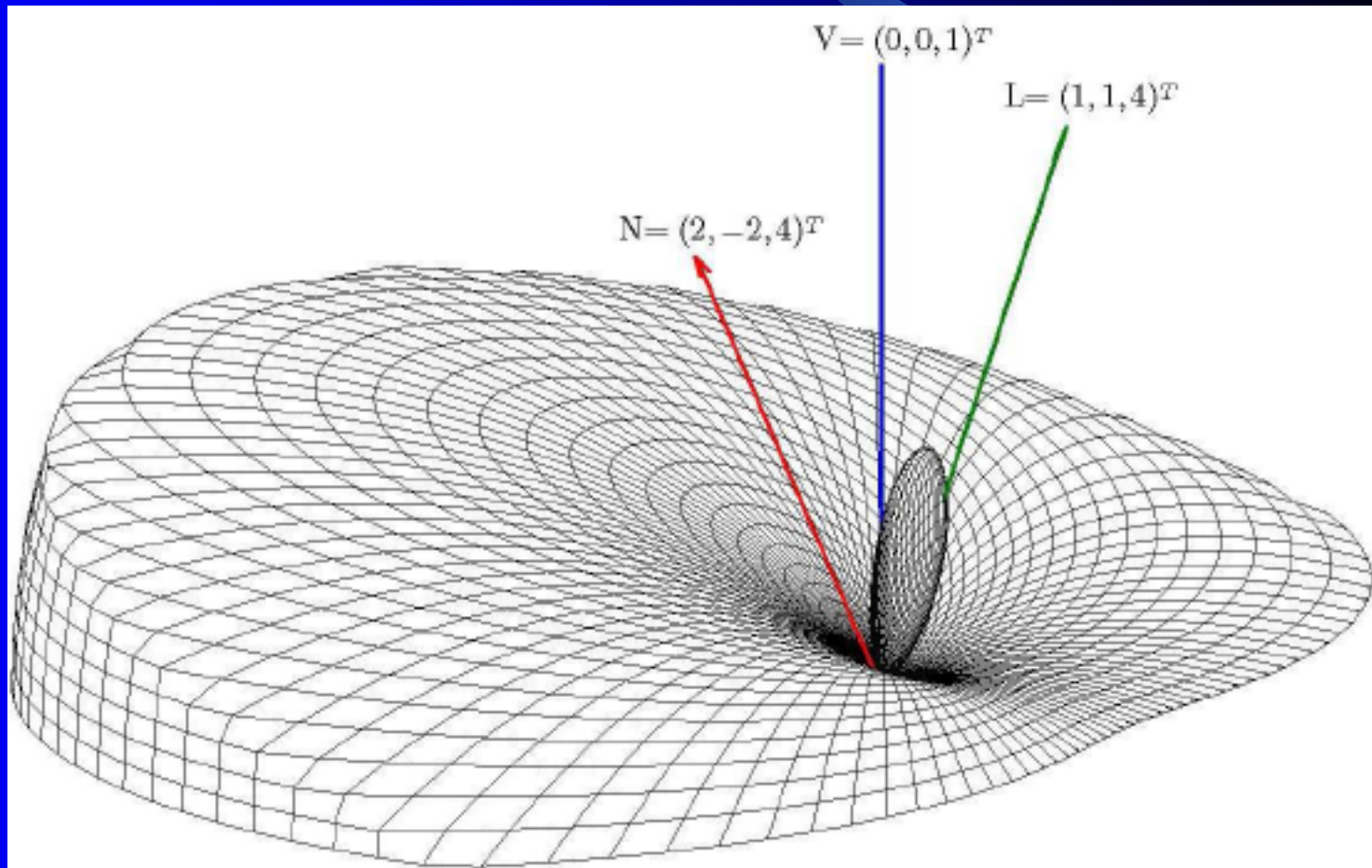
Minimising the Brightness Error

Lambertian:



Minimising the Brightness Error

Torrance and Sparrow:

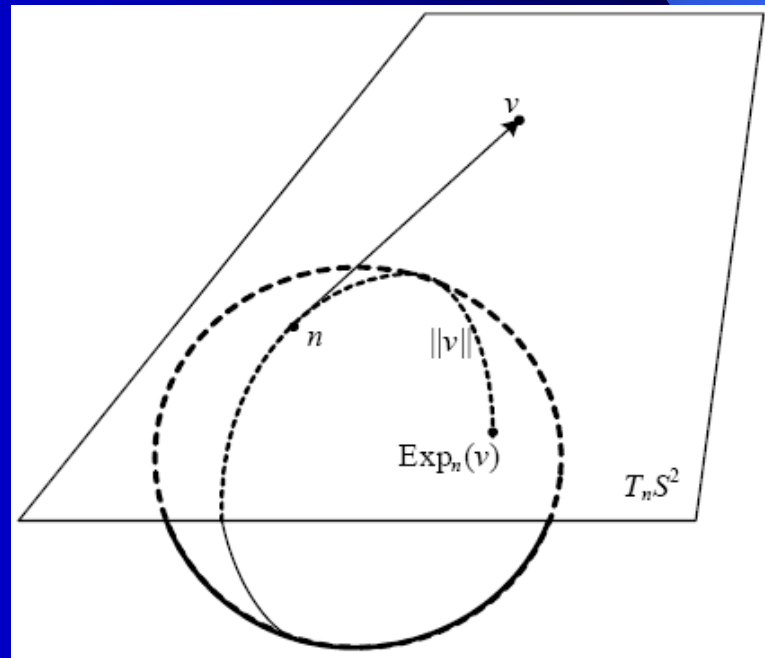


Minimising the Brightness Error

- Approximate gradient of brightness error function in terms of a vector on the tangent plane to the sphere:

$$\nabla f(n) = \left(\frac{f(\text{Exp}_n[(\epsilon, 0)^T]) - f(n)}{\epsilon}, \frac{f(\text{Exp}_n[(0, \epsilon)^T]) - f(n)}{\epsilon} \right)^T$$

Exponential map transforms points on tangent plane to points on sphere:



Minimising the Brightness Error

- Solve minimisation using gradient descent:

$$n_{t+1} = \text{Exp}_{n_t}(-\gamma \nabla f(n_t))$$

- 2 step algorithm generalises Worthington and Hancock algorithm to arbitrary reflectance models:

$$\begin{aligned} 1. \mathbf{n}'_t &= f_{\text{Reg}}(\mathbf{n}_t); \\ 2. \mathbf{n}_{t+1} &= \arg \min_{\mathbf{n}} \mathcal{E}_{\text{Bright}}(\mathbf{n}), \end{aligned}$$

- Step 2 is solved using gradient descent with result of step 1 as initialisation
- Critically dependent on choice of regularization constraint

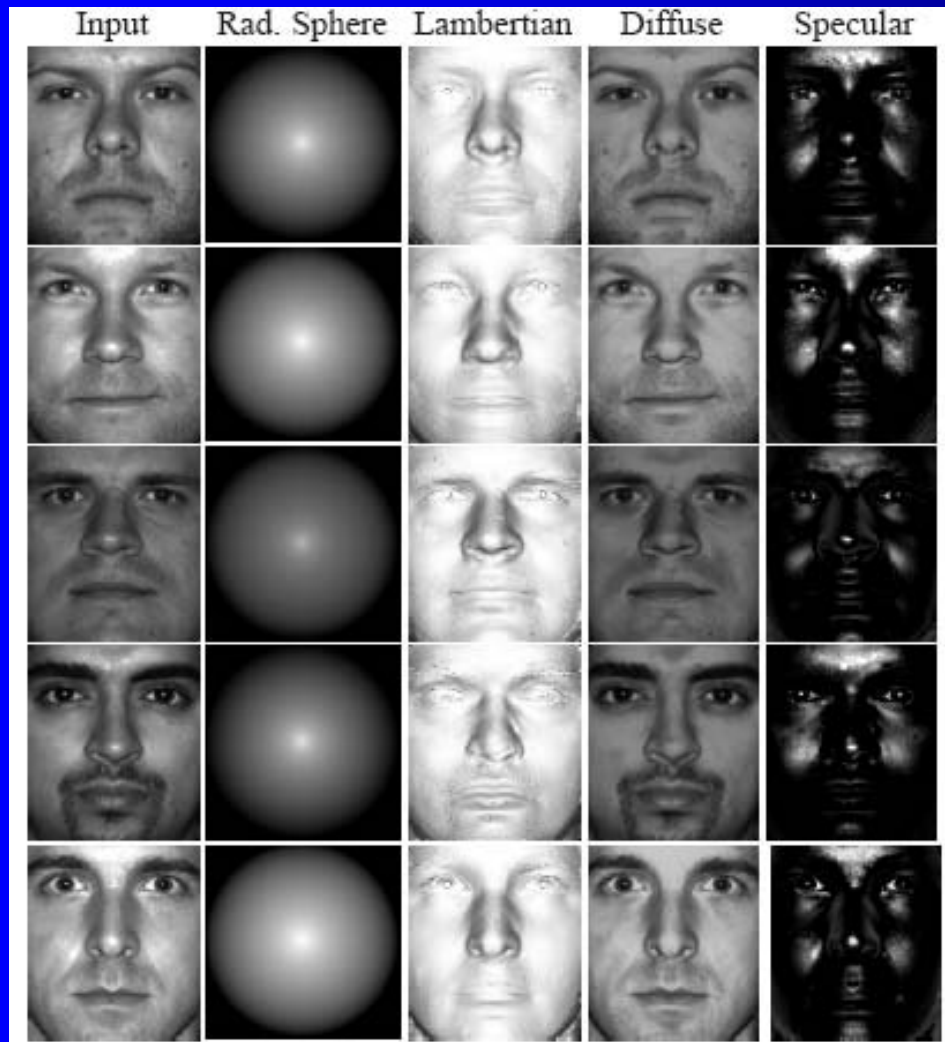
Reflectance parameters

L – Linear least squares

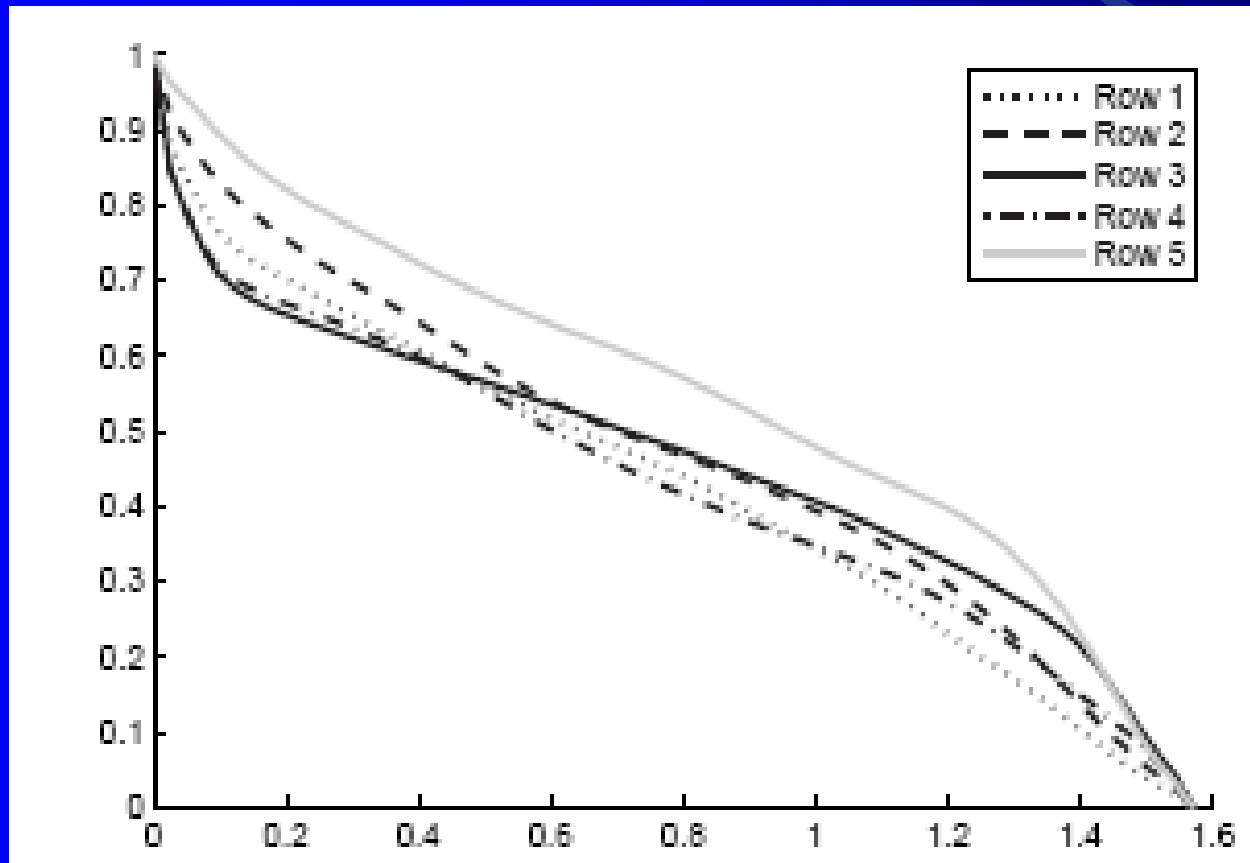
ρ_d – Rearrange radiance function. Solve for each pixel independently, i.e. spatially varying

ρ_s and v – Non-linear least squares. Fixed across image, i.e. specular reflectance assumed homogenous

Real world data



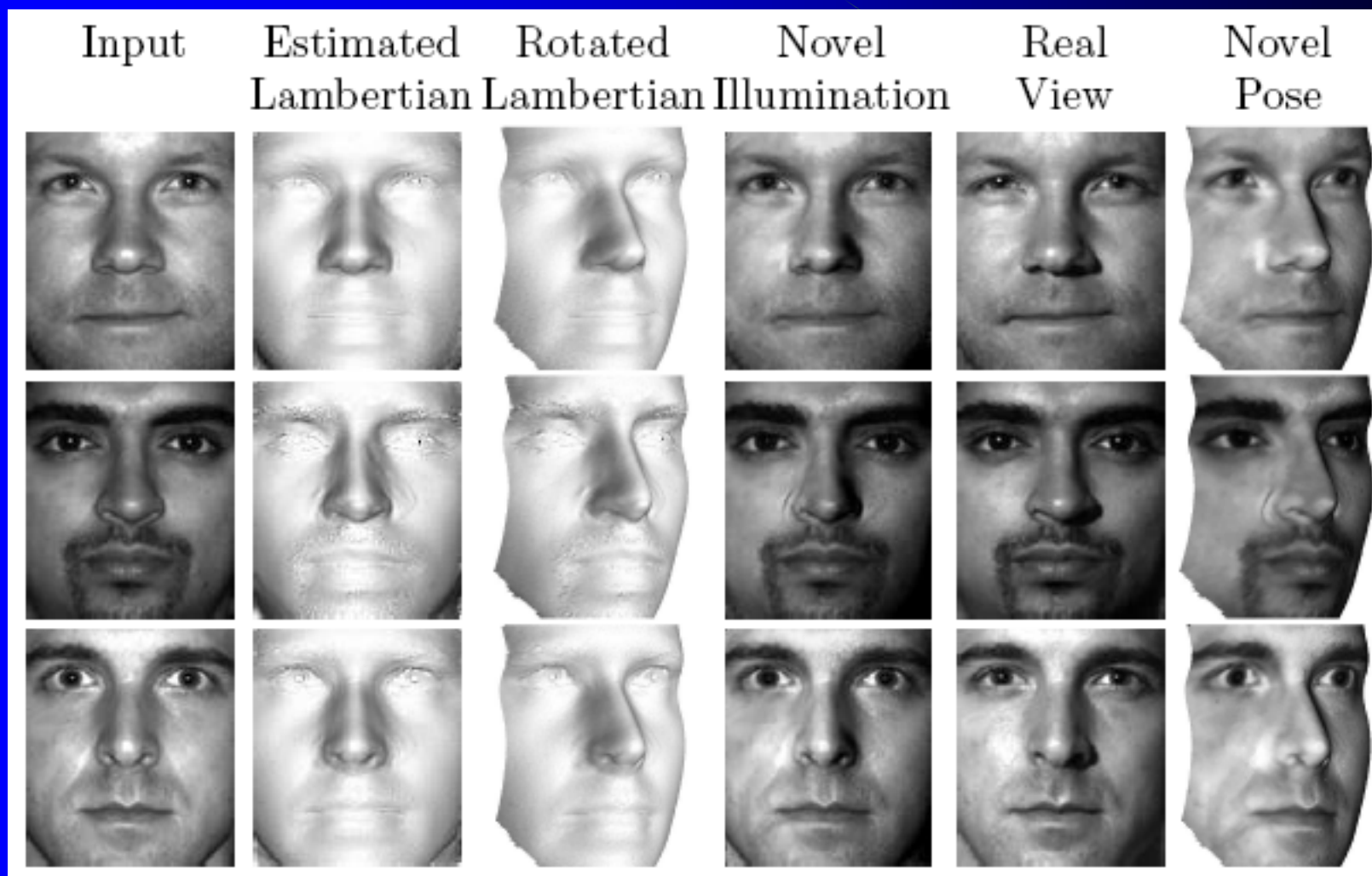
Estimated radiance function



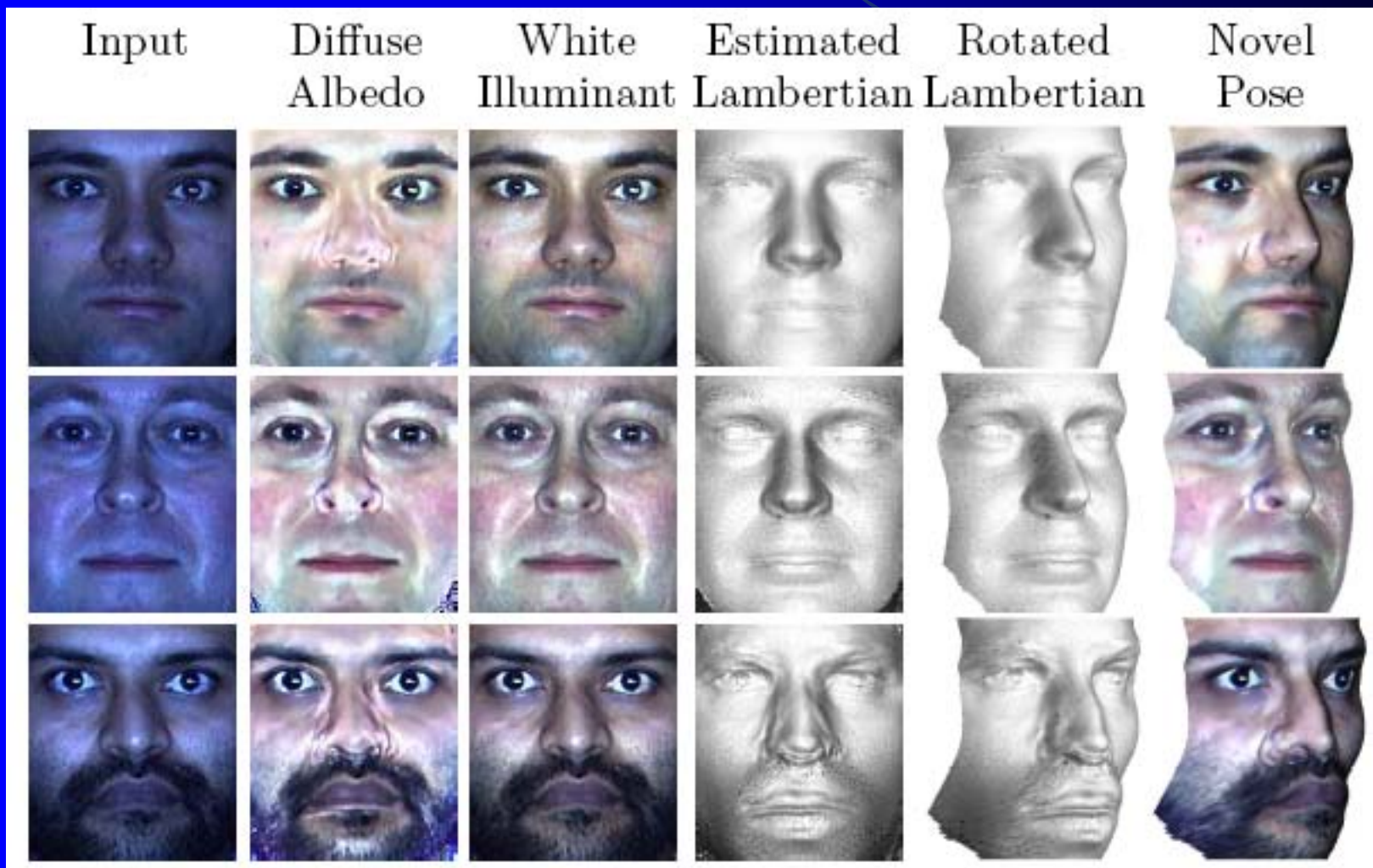
Synthesised views



Shape Recovery Results



Colour Shape Recovery Results



Non-frontal Illumination

Correcting for non-frontal illumination



Synthesising novel illumination (colour & direction)



Recognition

Gender determination using
weighted PGA

A decorative graphic element consisting of a blue gradient shape that starts as a thin wedge and expands into a larger, curved triangular form, pointing towards the bottom right corner of the slide.

- Method

- Gender classification using the parameterisation of fields of facial surface normals, a 2.5D shape representation.
- Facial surface normals are recovered from intensity images using non-Lambertian SFS.
- Associate a dissimilarity weight with each pairwise distances between labelled data to emphasize the interclass separation and improve the gender discriminating power of the leading principal geodesics.

Experimental Results

- Data
 - Ground-truth needle-maps: Max Planck database
100 female and 100 male range Images

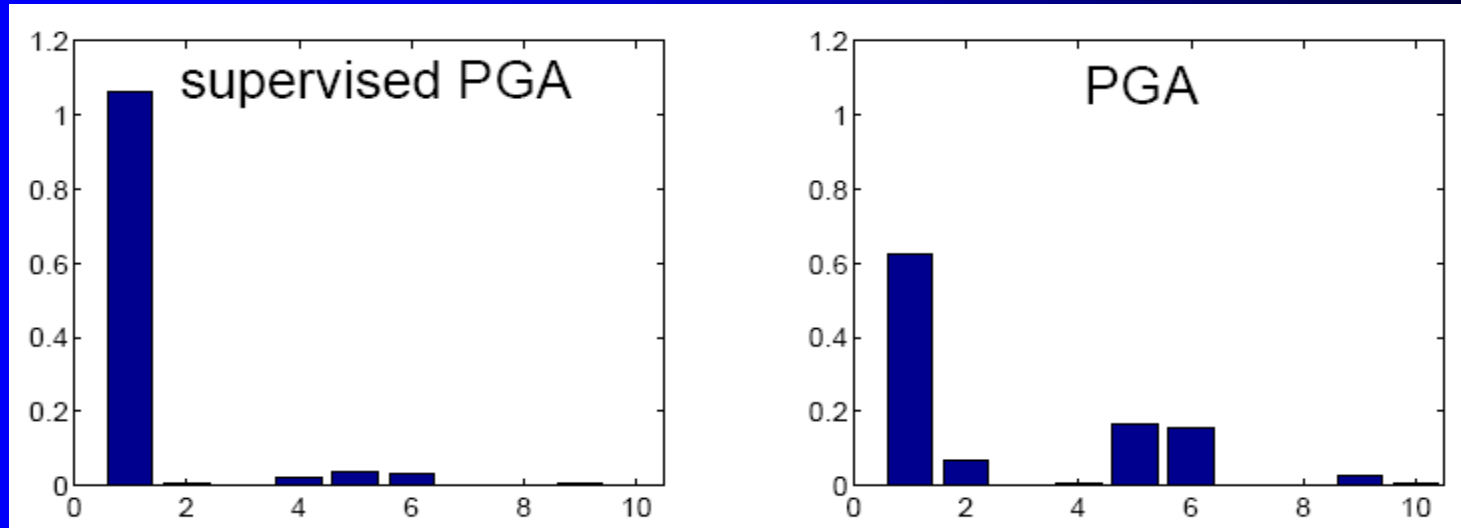


- Recovered needle-maps: non-Lambertian SFS on AR face database, 94 female and 74 male facial images

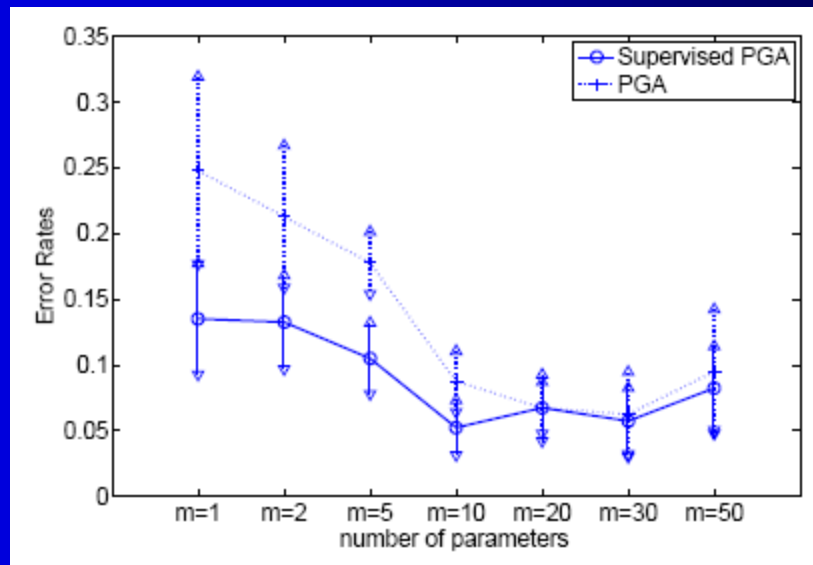


Results on ground-truth data

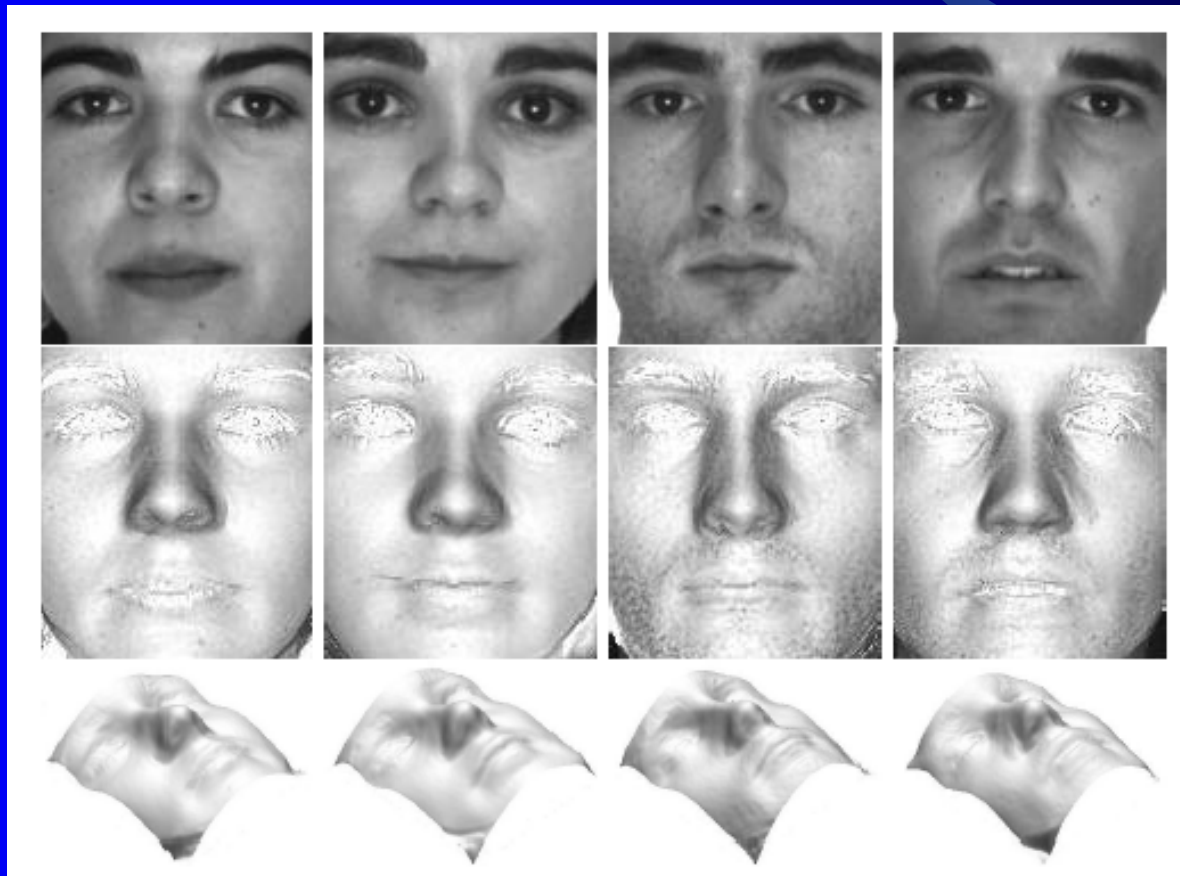
- Discriminating powers of leading 10



- Classification error rates

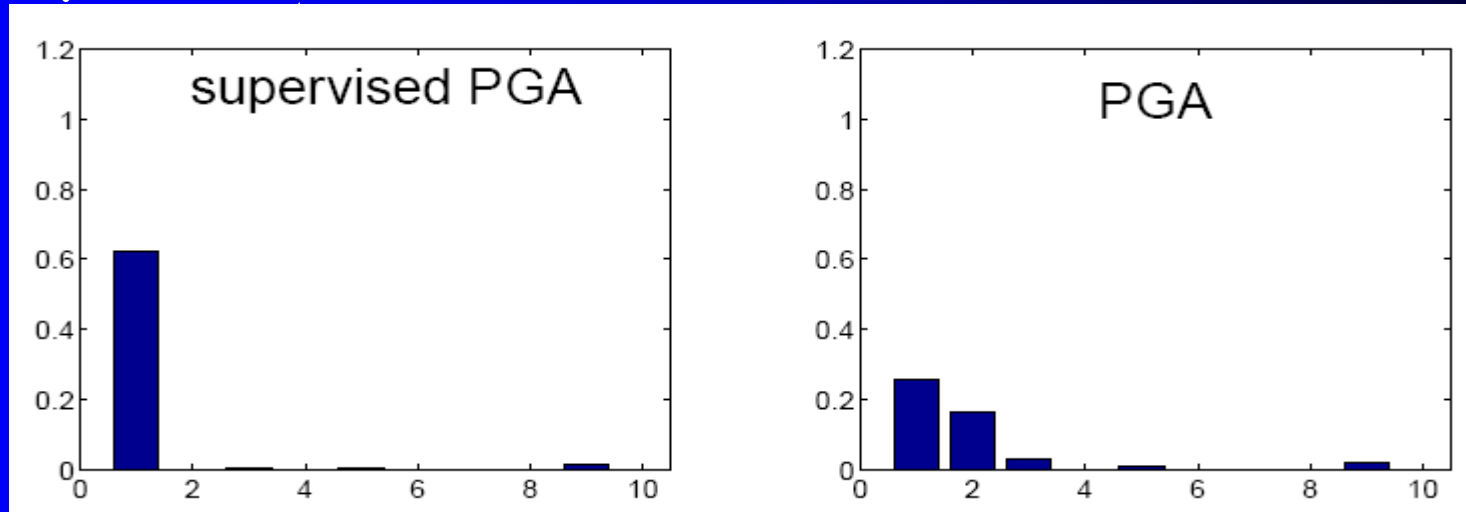


Performance of non-Lambertian SFS

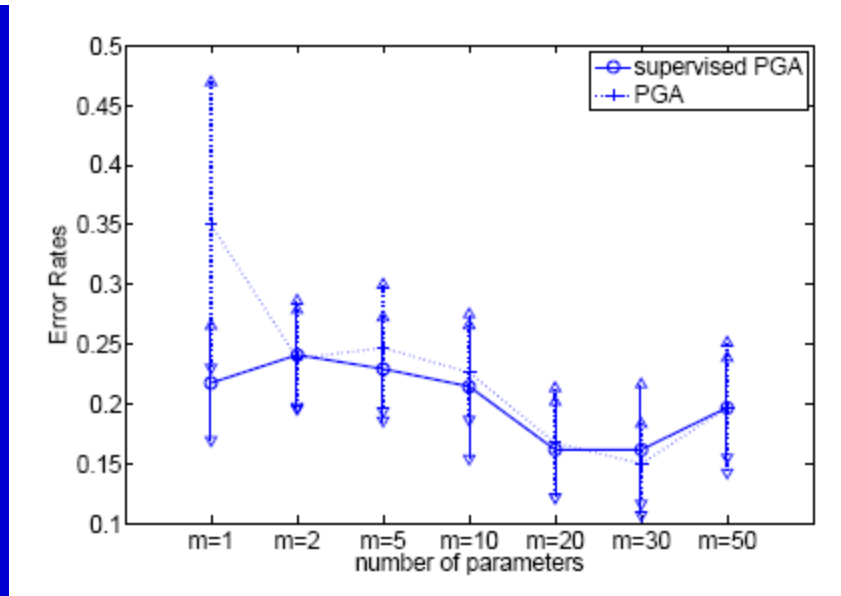


Results on brightness images

- Discriminating powers of leading 10



- Classification error rates

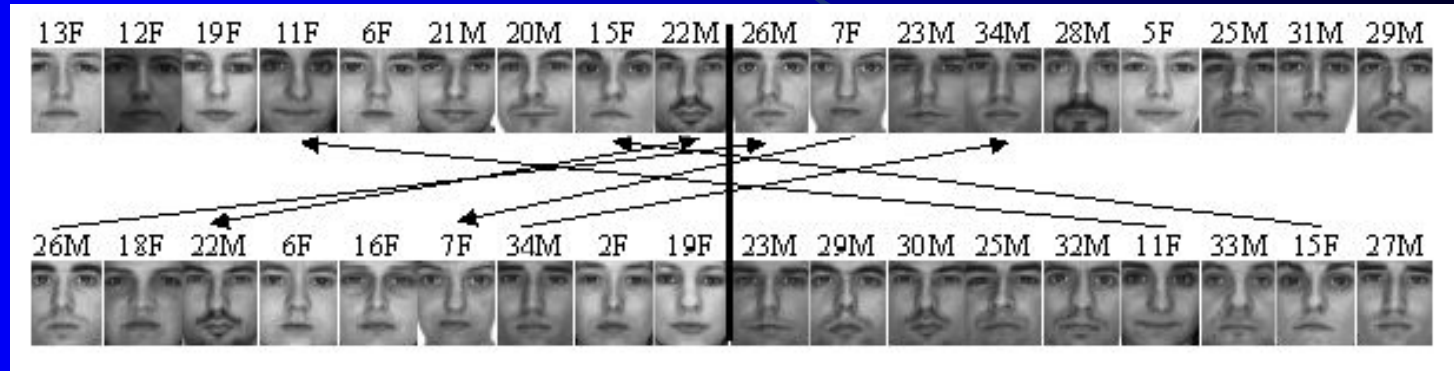


Results on brightness images

- Visualization of one classification

Supervised
PGA

Standard
PGA




- using supervised PGA, the misclassified faces (21M, 20M, 22M, 7F, 5F) are more concentrated in the overlapping area.
- Faces 26M, 34M, 11F and 15F which are misclassified using standard PGA, are correctly classified using supervised PGA

Future Work

- Investigate the distribution of the weight matrices. This may have some potential for unsupervised learning.
- Improve the non-Lambertian SFS method to recover more accurate facial shape.

Brain imaging study

Explore pose invariance in
recognition

A decorative graphic element consisting of a blue gradient shape that starts as a thin wedge and expands into a larger, curved triangular form, pointing towards the bottom right corner of the slide.

Full account of work

- Paper forthcoming in ``Cerebral Cortex'' 2008:

``The M170 Reflects a Viewpoint
Dependant Representation for both
Familiar and Unfamiliar Faces''

Outline

- Background: Cognitive model and regions of the brain.
- Computer vision: generation of stimuli.
- Magneto-encephalographic imaging: detect response to stimuli in M170 using SQUIDS positioned on cranium.
- Interpretation of results with familiar/unfamiliar face stimuli in different poses.

Background

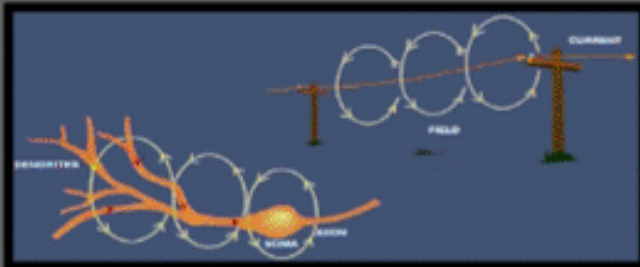
- **View dependant representations:** Logothetis, Bulthoff.
- **View invariant representations of face:** Young and Bruce.
- **Functional imaging studies:** face selective regions in occipital and temporal lobes. Face identity processing associated with inferior temporal lobe (face fusiform area) (Grill-Spector).

Magneto-encephalography

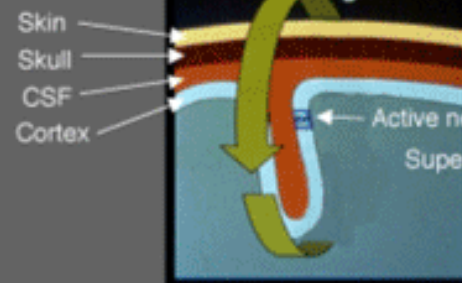
- Currents induced by neuronal activity in M170.
- Magnetic flux generated detected using SQUIDS placed on cranium.
- Good temporal resolution but poor spatial resolution.

Basic Principles of MEG

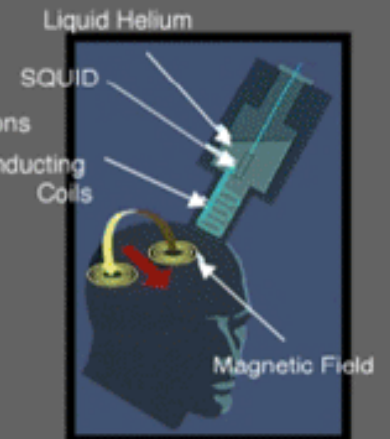
Sources of Magnetic Fields



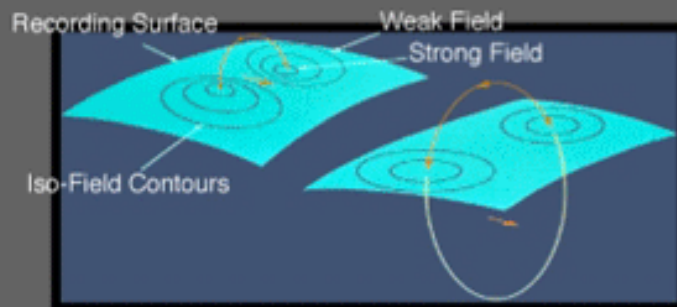
Orientation of Neurons



Detection Device



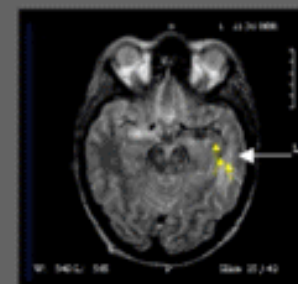
Magnetic Field Pattern



Model

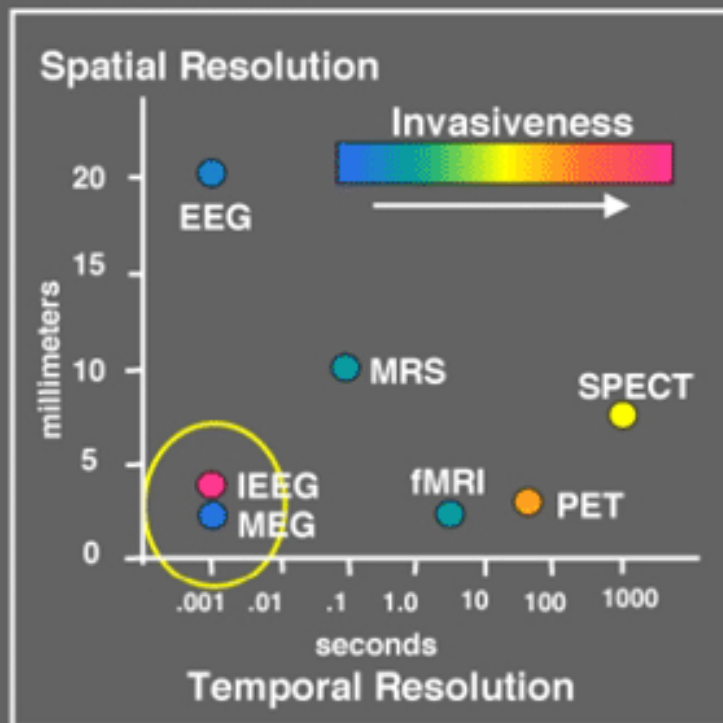


Result

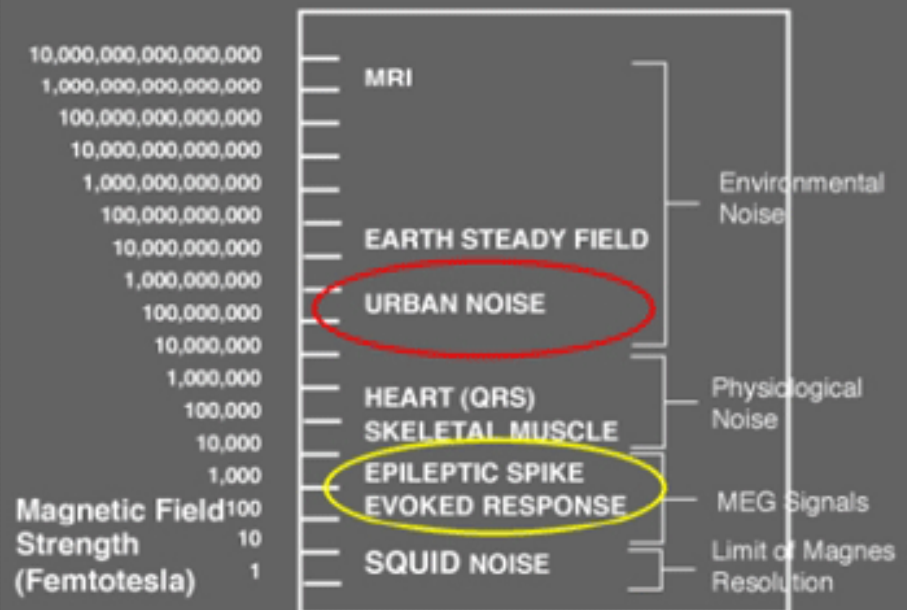


Properties of MEG

MEG Provides High Spatial and High Temporal Resolution

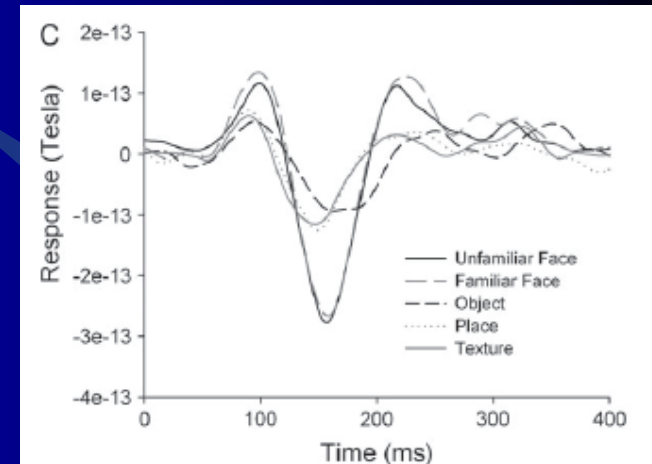


Strengths of Biological and Environmental Magnetic Fields



M170

- Face selective potential that correlates to successful face recognition.
- Delayed for inverted faces.
- Reduced for patients with prosopagnosia.



Generating stimuli

- Apply shape-from-shading algorithm (Smith and Hancock, PAMI 2006) to frontal images of faces with known light source direction.
- Recover facial shape (normal map and surface height function) together with albedo (texture) map.
- Generate novel views by rotating height surface and re-illuminating texture map with different light source directions.
- Familiar subjects are famous people (Blair, Bush, ClintonX2, Dench, DiCaprio, Clooney, etc).

Famous people



Questions to be answered

- Is M170 involved in the representation of identity?
- Does M170 reflect viewpoint dependant or viewpoint invariant representation of faces?
- Does M170 differ in response for familiar and unfamiliar faces?

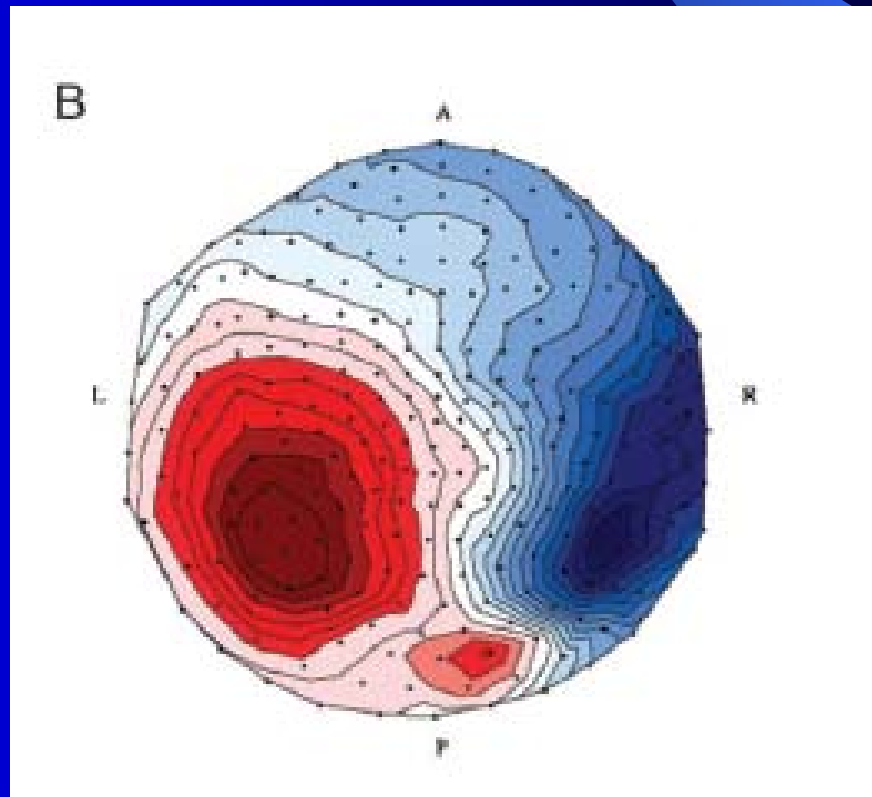
Experiment

- Subjects: 9 females and 9 males mean age 23 with good visual acuity.
- Localiser scans: determine which sensors respond to faces by presenting subjects with familiar faces, unfamiliar faces, inanimate objects, places and textures. Images presented in block of 25 (5 images from each category randomly ordered), each image presented for 400ms and screen blanked for 100 ms.
- Adaptation scans: Blocks of 12 familiar and unfamiliar faces. Poses were 0,2,4,6,4,2,0,-2,-4,-6,-4,-2,0 degrees in the different blocks.
- MEG: 248 channels, sampled at 1017.25 Hz. Subject to 1Hz high pass and 200Hz low pass cutoff.

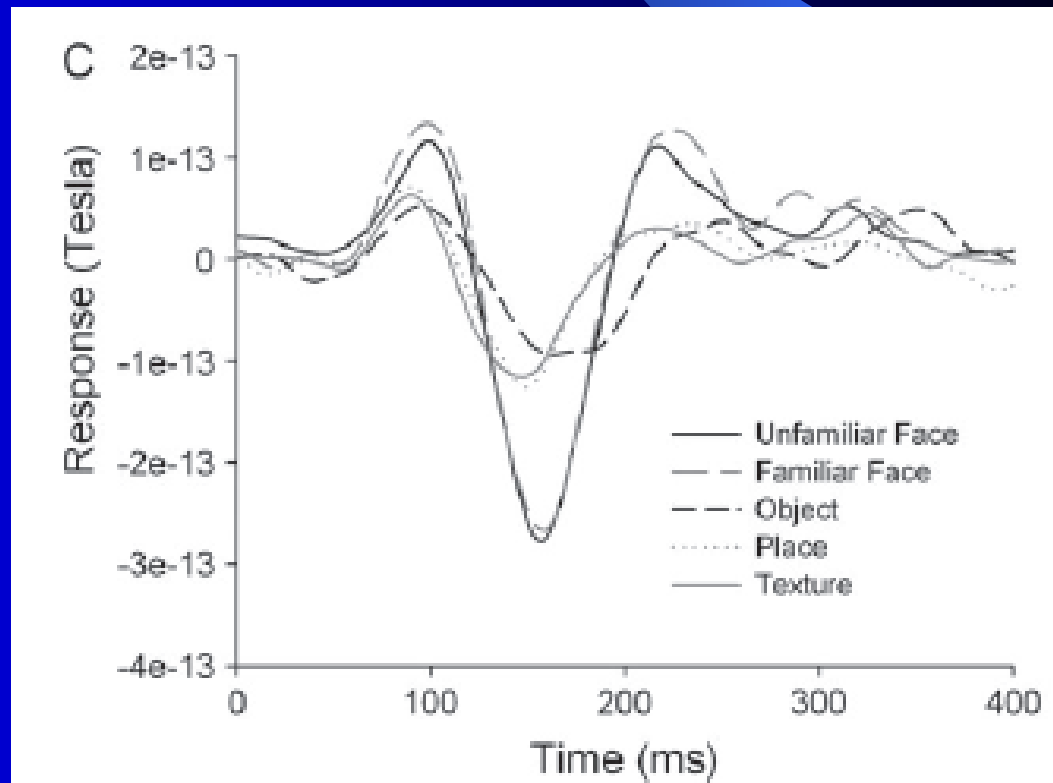
Localiser scan

- Locate occipital regions that have higher response to familiar/unfamiliar faces than to other objects. 18 subjects showed right-hemisphere M170 response. 12 showed additional left hemisphere response.
- Two way ANOVA analysis (category-hemisphere) of peak M170 amplitude shows significant effect of category, but not hemisphere, and no interaction between them.
- No difference in mean M170 response for familiar or unfamiliar faces.

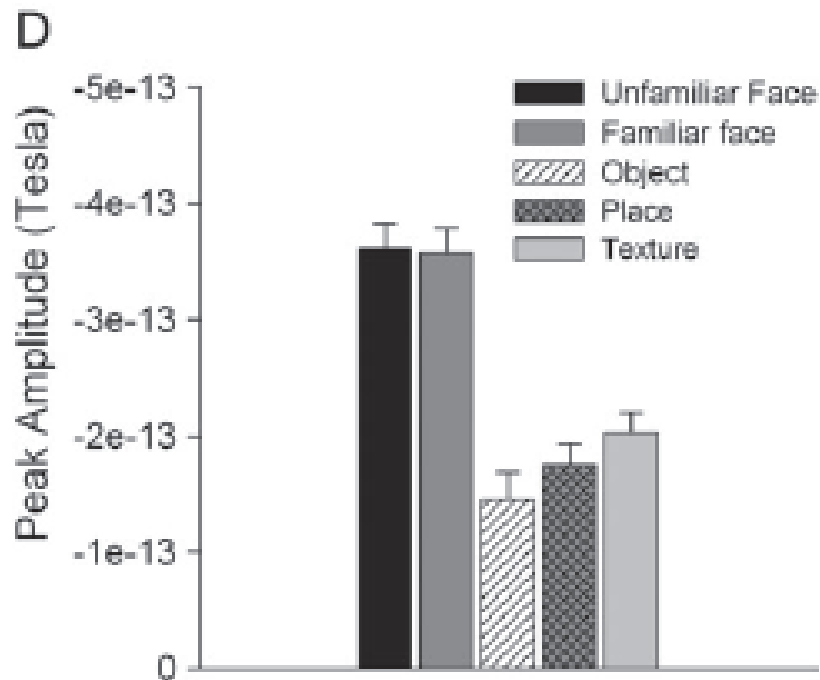
- MEG map for one subject: Response to unfamiliar faces 163ms after presentation of stimulus.



- Average MEG waveform for each object category in localiser scan.



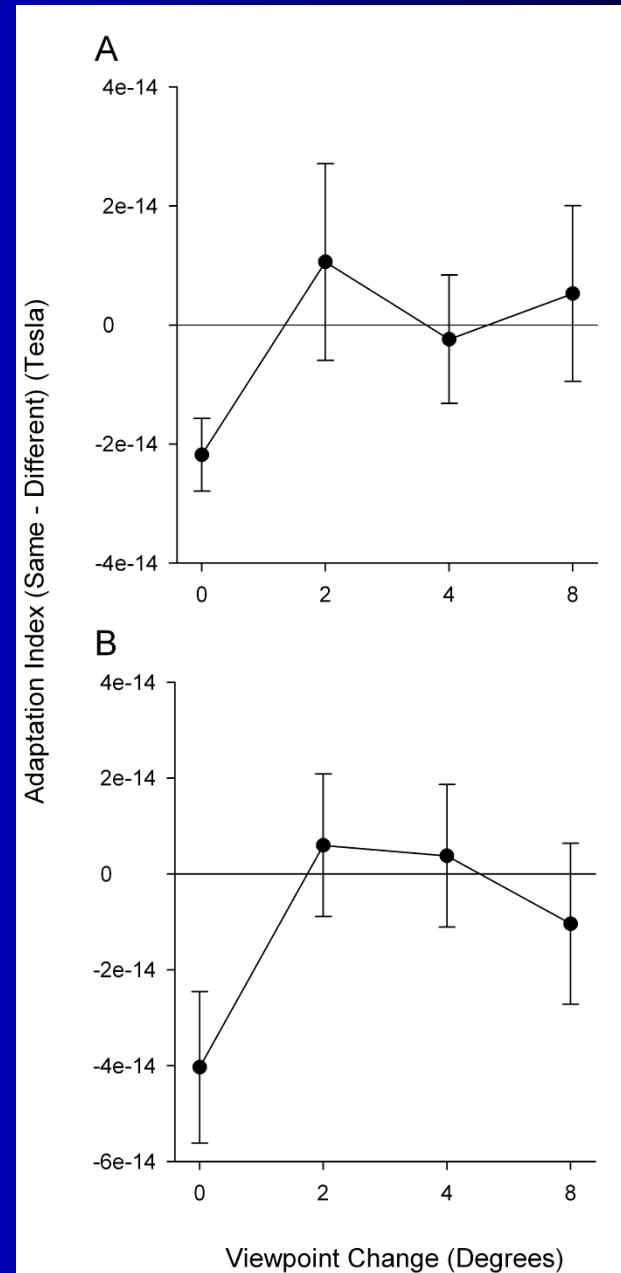
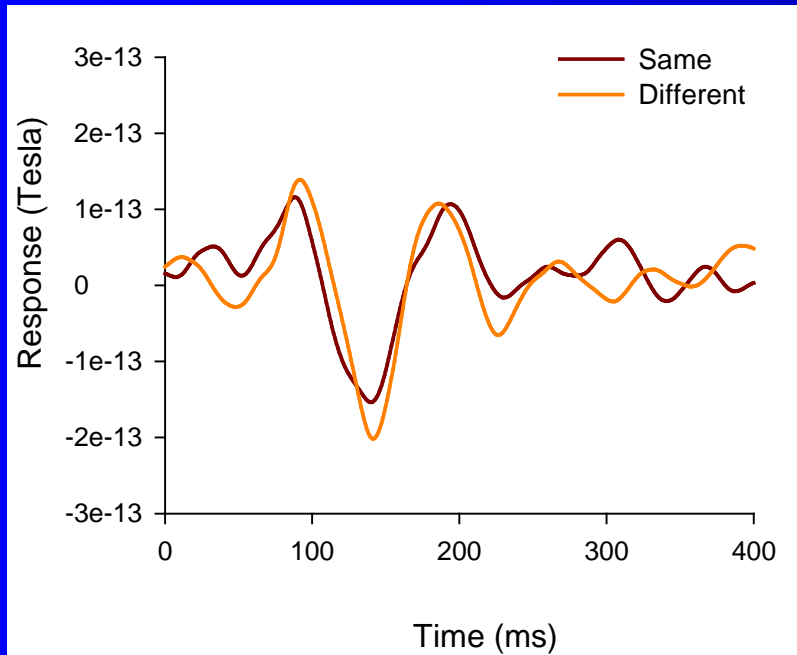
- Average peak MEG amplitude for each object category

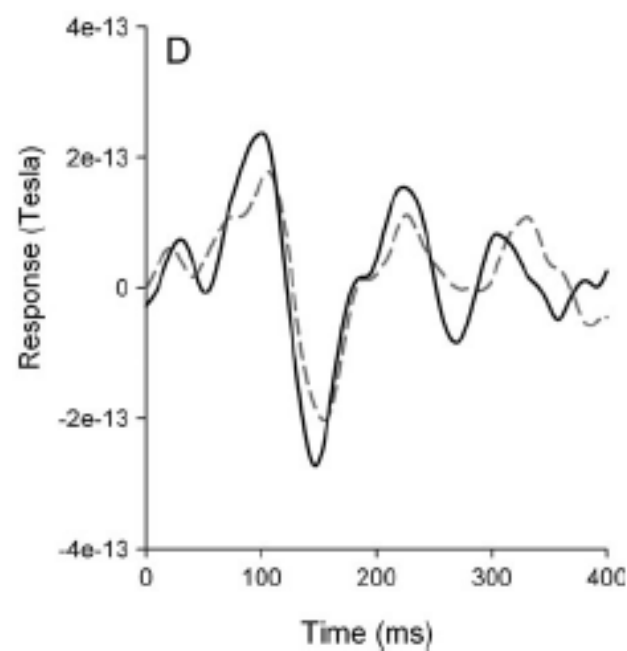
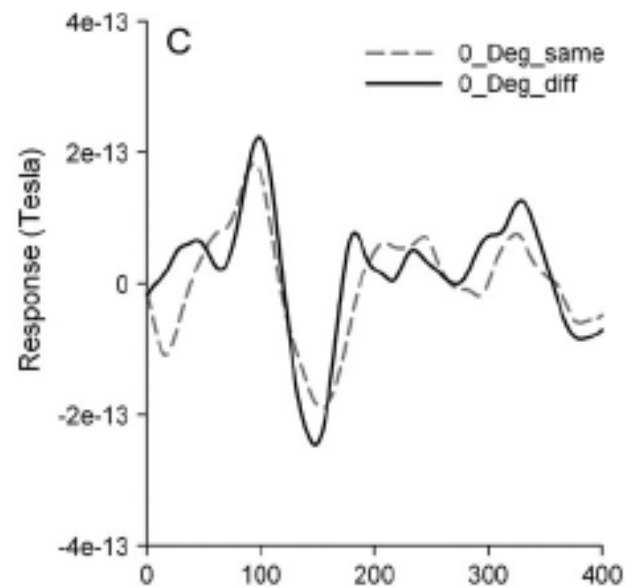
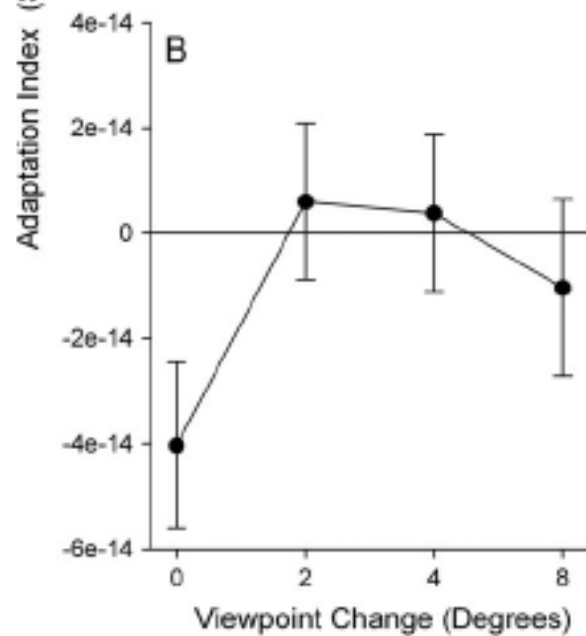
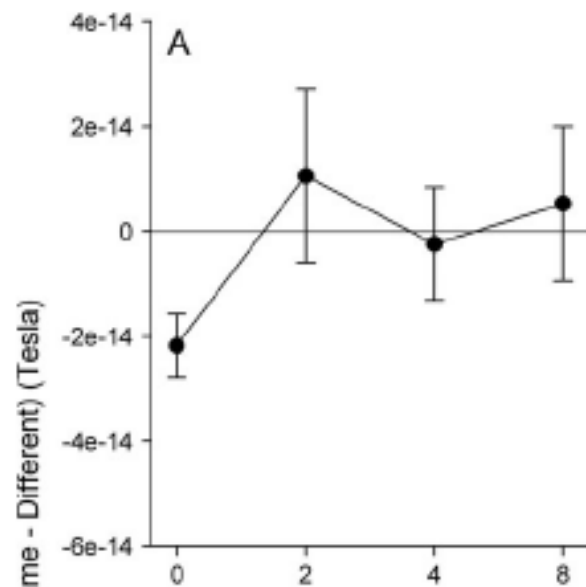


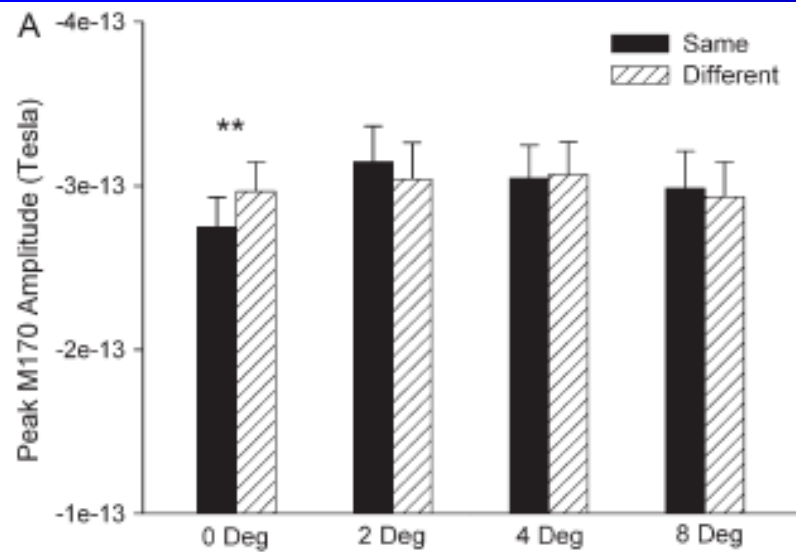
Adaptation scan

- Four-way (identity-hemisphere-familiarity-viewpoint) ANOVA showed no effect in any variable. However, significant interactions between hemisphere, identity and view.
- Three-way (identity-fame-viewpoint) showed significant effect of viewpoint and strong interaction between viewpoint and identity.
- M170 response for same and different unfamiliar faces with angles of 2, 4, and 8 degree angle changes showed no differences.

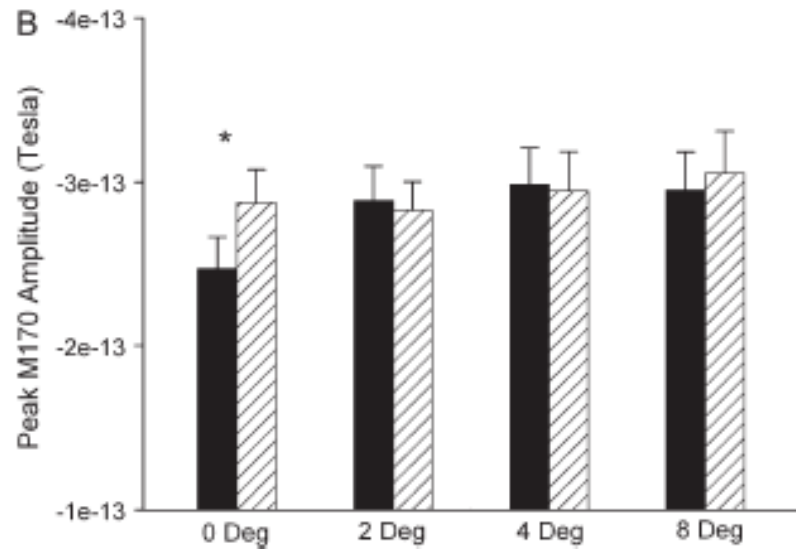
M170 ADAPATATION – VARY VIEWPOINT







A: unfamiliar faces



B: familiar faces

Figure 5. Bar graphs representing the average peak M170 amplitude in the right hemisphere across all subjects to (A) unfamiliar and (B) familiar faces with the same or different identity. Error bars represent ± 1 standard error. ****** $P < 0.01$, ***** $P < 0.05$.

Conclusions

- Have shown that M170 potential adapts to faces of the same identity if they are shown with the same viewpoints.
- Adaptation changes when viewpoint changes.
- Seems to support Logothetis/Bulthoff view dependant representation rather than Bruce/Young invariant representation.
- View invariant representation may take place at a later stage of processing.

The future

- Learn reflectance function as component part of coupled model. ARK+ERH have shown how learn radiance function using Gauss-map representation. Would fit well with EAP.
- Analytically understand link between surface normal and height eigenmodes, to facilitate better recovery of surface.